Cilia-mediated Hedgehog signaling controls form and function in the mammalian larynx

Jacqueline M. Tabler[1]*, Maggie M. Rigney[1]*, Gordon J. Berman[2], Swetha Gopalakrishnan[3], Eglantine Heude[3], Hadeel A. Al-lami[4], Basil Z. Yannakoudiadkis[4], Rebecca D. Fitch[1], Christopher Carter[1], Steven Vokes[1], Karen J. Liu[4], Shahragim Tajbakhsh[3], Roian Egnor[5], and John B. Wallingford[1]**

1. Dept. of Molecular Biosciences, University of Texas at Austin
2. Department of Biology, Emory University
3. Stem Cells & Development, CNRS UMR3738, Dept. of Developmental & Stem Cell Biology, Institut Pasteur, Paris.
4. Department of Craniofacial Development and Stem Cell Biology, King's College London
5. HHMI Janelia Research Campus

*These authors contributed equally.

**Corresponding author:
University of Texas
2401 Speedway
Austin, Tx. 78712
Wallingford@austin.utexas.edu
512-232-2784

Abstract:

Acoustic communication is fundamental to social interactions among animals, including humans. In fact, deficits in voice impair the quality of life for a large and diverse population of patients. Understanding the molecular genetic mechanisms of development and function in the vocal apparatus is thus an important challenge with relevance both to the basic biology of animal communication and to biomedicine. However, surprisingly little is known about the developmental biology of the mammalian larynx. Here, we used genetic fate mapping to chart the embryological origins of the tissues in the mouse larynx, and we describe the developmental etiology of laryngeal defects in mice with disruptions in cilia-mediated Hedgehog signaling. In addition, we show that mild laryngeal defects correlate with changes in the acoustic structure of vocalizations. Together, these data provide key new insights in the molecular genetics of form and function in the mammalian vocal apparatus.

Introduction

Vocal communication is fundamental to social interaction. Indeed, the voice is so crucial to our quality of life that the neurobiology of speech and language has been hotly studied for decades, as has the developmental biology of the ear. These bodies of work stand in surprising contrast to our still rudimentary understanding of the developmental biology of the organs of vocalization, the larynx and vocal folds. This is true despite the fact that most animal vocalizations, including human speech, are critically dependent upon careful control of airflow though the larynx. In fact, larynx and vocal fold morphology and elasticity are key factors influencing vocalization even in animals with widely divergent mechanisms of sound production (e.g. audible vocalizations in humans, ultrasound in rodents).

This deficit in our understanding of laryngeal and vocal fold development is significant, because many people who are capable of normal *speech* still cannot communicate due to defects in *voice* (e.g. problems with pitch, loudness, etc.). Some voice defects arise from acute insults, such as insufficient hydration of the vocal folds in *laryngitis sicca* or vocal fold hemorrhages resulting from blood vessel ruptures (Aronson and Bless, 2009). Other conditions are hereditary and chronic, such as those arising from mutations in

genes encoding the extracellular matrix protein Elastin (Vaux et al., 2003; Watts et al., 2008). All of these conditions impact the voice, thereby impacting patients' well-being.

A wide array of human birth defect syndromes also involve voice defects, and prominent among these are disorders stemming from failure of the Hedgehog (HH) signaling pathway, an evolutionarily conserved mechanism for cell-cell communication (Briscoe and Therond, 2013). For example, Pallister-Hall Syndrome is caused by mutations in *Gli3*, a key transducer of HH signals. These patients have hoarse and/or growling voices, and they frequently exhibit laryngeal clefts and bifid epiglottis (Hall et al., 1980; Tyler, 1985). Pallister-Hall Syndrome is known for its variable expressivity, and accordingly, this disorder is also associated with milder laryngeal anomalies (Ondrey et al., 2000). Importantly, laryngeal and voice defects are not limited to *Gli3* mutation, but have also been associated with mutation in the related factor *Gli2* (Franca et al., 2010), in the Shh transducer *Kif7* (Putoux et al., 2012; Walsh et al., 2013), and in *Shh* itself (Cohen, 2004).

Cilia are essential organelles for transduction of HH signals (Goetz and Anderson, 2010), and as a result, voice defects are also commonly associated with ciliopathies, human diseases that share an etiology of defective cilia structure or function (Hildebrandt et al., 2011). For example, a breathy, high-pitched voice is a diagnostic criterion for Bardet-Biedl and Oral-Facial-Digital syndromes, while hoarse voices are diagnostic for Joubert Syndrome (Beales et al., 1999; Garstecki et al., 1972; Hayes et al., 2008; Maria et al., 1999; Rimoin and Edgerton, 1967). Laryngeal defects such as laryngeal stenosis and bifid epiglottis are also common features of other ciliopathies (Carron, 2006; Hayes et al., 2008; Silengo et al., 1987; Steichen-Gersdorf et al., 1994; Stevens and Ledbetter, 2005).

Understanding the molecular genetic basis for voice disorders in human birth defect patients is not the only factor motivating a deeper study of laryngeal developmental biology. Indeed, vocal communication is ubiquitous in tetrapod animals, impacting a wide array of behaviors. For example, the Panamanian Tungara frog creates a complex, multi-tonal call that critically influences female mate choice, and this call requires a sexually dimporphic elaboration of the male larynx, the developmental basis of which is entirely unknown (Griddi-Papp et al., 2006; Ryan, 1990). So too is the morphology of

the songbird syrinx central to sound production, yet almost nothing is known of the developmental biology of this functional cognate of the larynx, despite the key role of bird song as a model for the study of acoustic communication. Likewise, the larynx of mice is central to their production of ultrasonic vocalizations throughout life. Despite the widespread use of mice for studies of developmental biology, the molecular genetics of mouse laryngeal development remain only cursorily poorly defined (e.g. (Bose et al., 2002; Lungova et al., 2015). Clearly, a deeper understanding of the molecular genetic basis of laryngeal patterning and morphogenesis will inform our understanding of vertebrate animal behaviors involving acoustic communication.

In mammals, the larynx and vocal folds are comprised of an elaborate mixture of cartilages, muscles, nerves, and connective tissue (Harrison, 1995; Henick, 1993; Lungova et al., 2015). The flanged circle of the cricoid cartilage, along with the C-shaped thyroid cartilage and intervening paired arytenoid cartilages provide the core of the laryngeal skeleton (Figure 1, blue, yellow, purple). Anchored to these are the vocal folds, which are in turn comprised of paired *cricoarytenoid*, *thyroarytenoid, cricothyroid* and *vocalis* muscles (Figure 1, pink, magenta, grey), as well as paired vocal ligaments (Figure 1, dark blue) and associated loose mesenchyme which we designate as the thyroglottal connective tissue (Figure 1, green). The general laryngeal structure is similar across the mammals (Harrison, 1995; Kaufman, 1992; Roberts, 1975a; Thomas et al., 2009), though rodents communicate most commonly in the ultrasonic range, using a mechanism for sound production that is distinct from that generating audible sound (Mahrt et al., 2016; Roberts, 1975b). Importantly however, diverse aspects of rodent ultrasound production parallel those of audible vocalizations in other mammals, including tight control of laryngeal muscle activity and mechanical properties of the vocal folds (Riede, 2011, 2013).

Here, we have characterized severe defects in laryngeal and vocal fold development in ciliopathic *Fuz* mutant mice, as well as similar though less severe defects in *Gli3* mutant mice. To understand the developmental trajectory of these defects, we first performed directed genetic fate mapping of the mouse larynx. We defined the embryonic origins for diverse tissues in the larynx, and also show that that laryngeal defects in both *Fuz* and *Gli3* mutants stem from an invasion of excess neural crest. Finally, we show that viable heterozygous *Gli3* mutant mice display quantitative changes in the morphology of the

vocal apparatus accompanied by significant changes in the acoustic structure of their ultrasonic vocalizations. Together, these findings provide an improved foundation for molecular genetic studies of development in the mammalian vocal apparatus, establish a genetic animal model for understanding human congenital laryngeal and voice defects, and demonstrate that excess neural crest is a common etiology underlying diverse Hedgehog-related craniofacial defects.

Results:

Laryngeal and vocal fold defects in mouse models of human ciliopathies and Pallister-Hall Syndrome:

Voice and laryngeal defects are common in ciliopathies, including Oral-facial-digital Syndrome Type 6 (Ref. (Hayes et al., 2008)). Recently, we showed that mutation of genes encoding the Ciliogenesis and Planar Cell Polarity effector (CPLANE) proteins results in OFD phenotypes in mice (Tabler et al., 2013; Toriyama et al., 2016). We therefore examined the larynx of mice lacking the CPLANE component *Fuz* as a first step towards understanding the developmental basis for ciliopathic larynx and voice defects. We observed severe malformation of the laryngeal cartilages in *Fuz* mice, as well as severely disorganized and hypoplastic vocal fold musculature (Figure 2A, B, -Figure 2-Figure Supplement 1B-C). No glottic space could be identified in the mutants, and the entire larynx was instead filled with an accumulation of loose connective tissue (Figure 2B, B', Figure 2-Figure Supplement. 1C-C). This severe derangement of the larynx in *Fuz* mutants prevented identification of specific laryngeal cartilages, making interpretation of these sections challenging. However, in frontal sections of control mice, we can identify four distinct cartilage elements (Figure 2-Figure Supplement 1A, B, B'), including the three laryngeal cartilages and the hyoid cartilage (Kaufman, 1992), while by contrast, we observe only what appears to be a single severely disordered cartilage element in similar frontal sections of *Fuz* mutants (Figure 2-Figure Supplement 1C, C').

Cilia-mediated Hedgehog signals influence the processing of both the Gli2 and Gli3 transcription factors (Haycraft et al., 2005), so we reasoned that mutation of either one of those two factors may generate milder, more interpretable laryngeal phenotypes. *Gli3*

mutant mice provide useful models for Gli-related human birth defects (Bose et al., 2002; Hui and Joyner, 1993), so we examined the *Gli3*$^{xt\text{-}J}$ mice. *Gli3* homozygous mutant mice developed with overt laryngeal defects, and as predicted, these were far milder than those in *Fuz* mice (Figure 2B, C). Unlike *Fuz* mutants, the laryngeal cartilages appeared normal in *Gli3* mutants and the glottis was evident. However, *Gli3*$^{-/-}$ mice consistently developed with an aberrant accumulation of Thyroglottal Connective Tissue (TgCT) around the vocal folds and particularly between the ventral limit of the glottis and the thyroid cartilage (Figure 2C, C', arrow), which was only 2-4 cells wide in normal mice, but was substantially expanded in *Gli3*$^{-/-}$ mice . In addition, we observed a decrease in the ventral extension of at least the *thyroarytenoid* muscles with a concomitant expansion of loose mesenchyme between these muscles and the thyroid cartilage (Figure 2C, C'). Interestingly, the accumulated mesenchyme in *Gli3* mutants appeared histologically similar to that seen in the more severely deranged larynx of *Fuz* mutants. Together, these data suggest a potential role for cilia-mediated Gli signaling in the patterning of the mammalian larynx.

Genetic fate mapping of the mouse larynx and vocal folds.

We next sought to understand the developmental trajectory of laryngeal defects in our mouse models, but this goal was hampered by the paucity of fate mapping data for the larynx. Indeed, there have as yet been only tangential reports of developmental origins of tissues in the larynx, and even these results are not entirely consistent. For example, one study reports that the major laryngeal cartilages are of a neural crest origin (Matsuoka et al., 2005), but that mapping is surprising in light of other mouse genetic studies that suggest a mixed lineage (e.g. (Jeong et al., 2004; Mori-Akiyama et al., 2003). Moreover, at least some laryngeal cartilages have a mesodermal origin in birds (Evans and Noden, 2006; Noden, 1986a). Recent studies using clonal or lineage analysis in mice suggests a relationship between some laryngeal muscles and the branchiomeric neck muscles (Gopalakrishnan et al., 2015; Lescroart et al., 2015), but information is lacking on the origin of the muscles and ligaments that comprise the vocal folds themselves.

We first used genetic fate mapping with *Wnt1*^{Cre}:*R26*$^{mT/mG}$ to map the descendants of neural crest cells in the larynx (Chai et al., 2000). Histological sections revealed distinct

lineages for the three laryngeal cartilages. While the thyroid cartilage was prominently labeled by *Wnt1^{Cre}::mGFP,* the arytenoid and cricoid cartilages were unlabeled, suggesting they are not crest-derived (Figure 3B). Strikingly, we observed a mixed lineage even within the single thyroid cartilage element; the medial caudal-most portion of the thyroid cartilage was consistently unlabeled by *Wnt1^{Cre}::mGFP* (Figure 3D, D', H, H'). This result was unexpected, so we confirmed it using an alternative promoter to label neural crest and an alternative reporter allele (Li et al., 2000). *Pax3^{Cre}:R26^{Tomato}* mice also displayed strong label throughout most of thyroid cartilage, but not in the caudal ventral midline; label was also absent from the cricoid and arytenoid cartilages (Figure 3 F-F').

We then performed a similar analysis using *Mesp1^{Cre};R26$^{mT/mG}$* and *Mesp1^{Cre};R26^{Tomato}* to map mesoderm-derived tissues (Saga et al., 1999) (Figure 4). *Mesp1^{Cre}* clearly labeled the ventral midline of the caudal thyroid cartilage, the region that was unlabeled b*y Wnt1^{Cr}; R26$^{mT/mG}$* (Figure 4C, D), arguing that this single cartilage arises from a mixture of neural crest and mesoderm. *Mesp1^{Cre};R26$^{mT/mG}$* and *Mesp1^{Cre};R26^{Tomato}* lineage analysis also revealed a mesodermal origin for the cricoid cartilage and arytenoid cartilages (Figure 4A,C).

In the vocal folds themselves, *Wnt1^{Cre}* drove GFP expression in the vocal ligaments, which are key elements for vocal fold apposition during sound production (Figure 3A, B, B'). Not surprisingly, the muscles of the vocal fold (*vocalis*, *thyroarytenoid)* were not labeled by *Wnt1^{Cre}::mGFP*, but were robustly labeled by *Mesp1^{Cre}* lineage (Figure 3A, B; Figure 4A, D). We also observed threads of *Wnt1^{Cre}* labeled, crest-derived cells interspersed within the vocal fold muscles (Figure 3A, B, B'). Some of these cells were identified as neurons by acetylated tubulin immunostaining (not shown), consistent with reports of vocal fold paralysis in neurocristopathies such as CHARGE syndrome (Jongmans et al., 2006; Siebert et al., 1985). Other crest-derived cells in the vocal fold likely represent the fascia separating the vocal muscles. Finally, *Wnt1^{Cre};R26$^{mT/mG}$* labeled the TgCT, the thin layer of connective tissue separating the ventral aspect of the glottis from the thyroid cartilage (Figure 3A, B).

Finally, because cranial and axial muscles develop *via* distinct genetic programs and originate from different mesodermal populations (Sambasivan et al., 2011), we sought to

246 determine which of the mesoderm lineages contributes to the muscles of the vocal folds.
247 In cranial mesoderm, *Isl1*-positive myogenic progenitors contribute to the formation of
248 head muscles (Harel et al., 2009; Nathan et al., 2008), while *Pax3*-positive cells in the
249 somitic mesoderm give rise to trunk and limb musculature. Analysis of the
250 *Pax3;R26*^{Tomato} lineage suggested that the muscles of the vocal folds, marked by Desmin
251 immunostaining, were not *Pax3*-derived and, thus, not of somitic origin (Figure 3F). In
252 contrast, *Isl1*^{Cre};*R26*$^{mT/mG}$ mice showed that all muscles of the vocal folds labeled by the
253 Desmin immunostaining (Figure 4A) were derived from the *Islet1; R26*$^{mT/mG}$ lineage
254 (Figure 4B), demonstrating their cranial mesoderm origin.
255
256 Together, these data complement previous lineage analyses of the larynx in other
257 species such as birds (Evans and Noden, 2006; Noden, 1986a) and provide the first
258 comprehensive description of the developmental origins of tissues in mammalian larynx.
259
260 **Excess neural crest underlies defective vocal fold morphogenesis in *Gli3* and *Fuz***
261 **mutant mice.**
262
263 Our fate mapping of the normal mouse larynx provided us with a platform from which to
264 explore the developmental basis for laryngeal defects in our mutant mice. To this end,
265 we performed *Wnt1*^{Cre} lineage labeling on *Fuz*$^{-/-}$ and *Gli3*$^{-/-}$ mice, focusing on cell
266 lineages during initial morphogenesis of the larynx. Between E11.5 and E14.5, laryngeal
267 morphogenesis proceeds in a surprisingly convoluted manner, with the previously patent
268 lumen of the developing trachea becoming occluded by the formation of a structure
269 known as the epithelial lamina. This epithelial lamina and tissues surrounding it then
270 remodel into the vocal folds, and a new lumen forms that will ultimately constitute the
271 glottis (Henick, 1993; Lungova et al., 2015; Sanudo and Domenech-Mateu, 1990). At
272 E14.25, when the re-canalized glottis is already apparent in control mice, we found that
273 condensing *Wnt1*^{Cre} labeled neural crest cells were present at the site of the future
274 thyroid cartilage and also in dorsally projecting streams presaging the neural crest-
275 derived tissues in the vocal folds, such as ligaments, fascia and neurons, while other
276 structures such as precursors of arytenoid and cricoid cartilage and future vocal fold
277 muscles were unlabeled (Figure 5A).
278

At these stages, the entire region of the forming larynx in *Fuz*$^{-/-}$ mice was filled with *Wnt1*^{Cre}*; R26*$^{mT/mG}$ positive, neural crest-derived cells; only scattered, individual unlabeled cells were observed (Figure 5B), consistent with the very severe phenotype observed at later stages by H&E staining (Figure 2B). *Gli3*$^{-/-}$ mice displayed less severe phenotypes, with a substantial reduction of the glottic space accompanied by a striking excess of *Wnt1*^{Cre}*; R26*$^{mT/mG}$ positive cells ventral to the glottis, in the area of the thyroid cartilage and TgCT (Figure 5C).

Fuz mutant mice rarely survive to E17.5, but at this stage in *Gli3*$^{+/-}$ *and Gli3*$^{-/-}$ mice, *Wnt1*^{Cre} lineage mapping revealed a continued excess of neural crest-derived cells that were concentrated around the periphery of the glottis compared to controls (Figure 6). The accumulation of *Wnt1*^{Cre}*; R26*$^{mT/mG}$ positive cells was especially pronounced in the TgCT separating the ventral edge of the glottis from thyroid cartilage in *Gli3*$^{-/-}$ embryos (Figure 6A, C). An excess of neural crest-derived cells was also observed to disrupt the normal close association of the vocal muscles with the thyroid cartilage (Figure 6C, C'). These excess neural crest cells were found precisely in the position occupied by the aberrant mesenchyme observed by H&E staining in *Gli3*$^{-/-}$ mutants (Figure 2C; Figure 6D', F'), indicating that the cells are neural crest-derived.

These findings suggest that expanded neural crest disrupts laryngeal morphogenesis, which is of interested because we previously showed that an expansion of neural crest underlies palate defects in *Fuz* mutant mice and skull defects in both *Fuz* and *Gli3* mutant mice (Tabler et al., 2013; Tabler et al., 2016). In those instances, the defects can be rescued by genetic reduction of *Fgf8* gene dosage (Tabler et al., 2013; Tabler et al., 2016). To ask if a similar mechanism acts in the larynx, we reduced the genetic dosage of *Fgf8* in *Fuz* mutants using the *Fgf8*^{LacZ} knockin allele (Ilagan et al., 2006). Analysis of frontal sections revealed a partial rescue of *Fuz* mutant phenotype when *Fgf8* gene dosage is reduced; while the glottis remained absent in *Fuz*$^{-/-}$*Fgf8*$^{+/LacZ}$ mice, overall anatomy was improved, as cricoid and arytenoid cartilage elements could be identified (Figure 2-Figure Supplement 1D, D'). We also previously found that the high arched palate phenotype of *Fuz* mutant mice results from effects prior to neural crest specification, because mice with specific deletion of *Fuz* using a conditional allele driven in neural crest by *Wnt1*^{cre} do not display high arched palate (Tabler et al., 2013).

Likewise, we find here that laryngeal morphogenesis is largely normal in *Fuz*$^{flox/-}$;*Wnt*$^{Cre/+}$ mice (Figure 2-Figure Supplement 2). Together, ……

Gli3^{xt-J} mutant mice display dose-dependent defects in laryngeal morphogenesis

The morphology of the larynx and vocal folds is complex, so in order to assess even subtle phenotypes in our mutant mice, we adapted a strategy of laryngeal morphometrics previously applied to human larynges (Eckel and Sittel, 1995). First, we quantified the morphology of the vocal folds themselves by measuring the cross sectional area occupied by the larynx, vocal muscles, and the *Wnt1*^{Cre} labeled vocal ligaments (Figure 7A,B, C). Consistent with the observed excess neural crest discussed above, we detected a significant increase in the area occupied by the vocal ligament (Figure 7C). We observed no corresponding increase in vocal muscle area, resulting in a significant change in the ratio of the area occupied by vocal ligament to that occupied by vocal muscles (Figure 7D). Strikingly, these phenotypes were dose dependent, with heterozygotes being significantly different from both wild-type and homozygotes (Figure 7C, D).

Next, we quantified the expansion of the TgCT by measuring the maximum distance between the dorsal edge of the thyroid cartilage and the ventral epithelial lining of the glottis (Figure 7A, E). Again, we observed a dose-dependent increase in this metric from wild-type to *Gli3*$^{xt-J}$ heterozygote to *Gli3*$^{xt-J}$ homozygotes (Figure 7E). The increase in connective tissue was observed along the length of the AP axis of the larynx in mutants, as evident in H&E stained sagittal sections of the larynx (Figure 6D'-F').

Finally, we measured the area of the glottic opening, which was significantly reduced in homozygous animals compared to controls, but was not changed in heterozygous animals (Figure 7F). Together, these data demonstrate that heterozygous *Gli3*$^{xt-j}$ mutant mice display a milder version of the same laryngeal phenotype observed in the homozygotes.

The acoustic structure of ultrasonic volcaizations is altered in heterozygous _Gli3_$^{xt/+}$ mutant mice.

Ultimately, vocalizations are the functional output from the larynx and vocal folds, which manifests as audible speech in humans and as audible and ultrasonic cries in mice. Throughout life, mice use a variety of ultrasonic vocalizations (USV), from pup isolation calls to adult courtship displays (Holy and Guo, 2005; Neunuebel et al., 2015; Noirot, 1966; Sewell, 1970; Zippelius and Schleidt, 1956). Because *Gli3*$^{xt/+}$ heterozygous mice are viable and display mild defects in laryngeal morphology (above), we examined recordings of pup isolation calls for evidence of altered vocalization. We analyzed over 9000 vocalizations from 5 wild type (4718) and 6 heterozygous (4295) mouse pups (see Figure 8A and B for example spectrograms), finding no significant differences in vocalization duration ($F_{1,9}$=3.88, p=0.08) and mean frequency ($F_{1,9}$=0.12, p=0.73), but a significant difference in bandwidth ($F_{1,9}$=12.22, p=0.007) (Figure 8C-E).

Mouse USVs are known to be highly variable (Heckman et al., 2016), and it was unclear *a priori* what features of vocalizations might be modified, therefore in addition to measures of basic acoustic properties, we used an analysis method that takes into account the entire structure of the vocal repertoire to ask if subtler differences in vocal phenotype might be present in our mutant mice. From our 9000+ calls, we constructed a map of the vocal repertoire space in which vocalizations with similar frequency contours occupy adjacent regions in the map (Figure 9A-C; see Material and Methods for details). In this map, simple calls lacking abrupt and discontinuous changes in frequency (frequency steps) cluster in the central body of the map, while more complex vocalizations with obvious frequency steps are distributed in “islands” or “peninsulas” surrounding the central body (Figure 9C).

This analysis revealed that the vocal repertoires of the two genotypes differed, and this difference was significant at multiple map locations (Figure 9D-F). While heterozygous *Gli3* mutant pups were capable of producing the full range of vocalizations made by control mice, they were significantly less likely to produce vocalizations with abrupt frequency steps (Figure 9E, F, warm colors), which is consistent with the observed reduction in overall vocal bandwidth in the mutant mice (Figure 8D). In our map, vocalizations in the same map area are acoustically similar, and so differences in the map between genotypes represent differences in acoustic structure between the genotypes; however, relative distance in the map beyond local relationships cannot be

interpreted. For example, the vocalizations in the map area with n=549 vocalizations differs from the vocalizations in the map area with n=763 only by the presence or absence of a small initial high frequency component (present in n=549, absent in n=763). Whether this acoustic distinction is behaviorally relevant is as yet unknown.

To test more directly for differences in the number of step and non-step vocalizations between WT and *Gli3*$^{xt/+}$ each vocalization was labeled as a step or non-step based on their position in the vocal repertoire map (see Figure 9C, vocalizations in green regions were labeled step, vocalizations in the pink region were labeled non-step). We found that 69% of control vocalizations had steps (3257/4718) versus only 48% of mutant vocalizations (2073/4295). Conversely, mutant pups produced a far higher proportion of calls without steps (Figure 9E, warm colors). This difference in the proportion of step vocalizations was highly significant (chi2=400.42, df=1, p<0.0001). In sum, *Gli3*$^{xt/+}$ heterozygous mice, display both morphological defects in the larynx and changes in their patterns of vocalization acoustics. While the acoustic structure of vocalizations is governed not only by the larynx, but also by the structure of the palate and pharynx, as well as neural inputs, our data nonetheless suggest that the mouse can provide a model for studying the links between laryngeal and voice defects in cilia and Gli-related craniofacial syndromes.

Discussion:

Despite the fundamental role of the larynx and vocal folds in mammalian communication, we still understand little about the molecular genetic control of their development. Here, we have explored the developmental basis for severe laryngeal defects in the ciliopathic *Fuz* mutant mice, and we describe qualitatively similar laryngeal defects, as well as vocalization defects, in mice mutant for the HH signal transduction protein *Gli3*. While we cannot rule out the possibility that *Fuz* loss may impact additional signaling activities, one parsimonious interpretation is that in the absence of *Fuz*, defective ciliogenesis leads in turn to defective Gli3 processing and disrupted HH signaling. Indeed, the key function of *Fuz* in both mice and frogs is the control of ciliogenesis (Gray et al., 2009; Park et al., 2006), and while Fuzzy controls PCP in *Drosophila* (Collier and Gubb, 1997), *Fuz* appears not to govern PCP-dependent proceses in mice (Heydeck and Liu, 2011).

Second, we have shown in *Fuz* mutant mice that both Gli3 processing and HH target gene expression are disruted in the head during stages of neural crest cell specification and patterning (Tabler et al., 2013). Similar results have been reported for the limb and neural tube (Gray et al., 2009; Heydeck et al., 2009). Third, Gli3 is a known transducer of HH signals, and we recently showed that *Fuz* and *Gli3* mutant mice share a common phenotype of an enlarged crest-derived frontal bone in the skull (Tabler et al., 2016). That result in the skull parallels what we observed here in the larynx: A severe defect arising from excess neural crest in *Fuz* mutants and a milder, but qualitatively similar, defect in the HH transducer *Gli3*. Combined with a central role for cilia in HH signal transduction (Goetz and Anderson, 2010), we feel the most parsimonious interpretation is that cilia-mediated HH signaling defects in *Fuz* mutants alter laryngeal morphogenesis.

Our data therefore support a model in which the expansion of laryngeal neural crest in *Fuz* mutants is a consequence of increased neural crest cell numbers at specification stages caused, ultimately, by expanded *Fgf8* expression. This conclusion is supported by our previous findings of increased neural crest cell numbers at E9 in Fuz mutant mice, as well as by our observation of excess *fgf8* gene expression in these mutants (Tabler et al., 2013) and by the finding in chick that Fgf8 can control neural crest cell numbers (Creuzet et al., 2004). Moreover, because *Fuz* is required for Gli3 processing (Heydeck et al., 2009; Tabler et al., 2013), our data are consistent with previous observations of expanded *fgf8* gene expression in *gli3* mutant mice (Aoto et al., 2002). Together, data presented here and in our previous studies (Tabler et al., 2013; Tabler et al., 2016) suggest that expanded neural crest is a unifying embryological mechanism for palate, skull and larynx defects in ciliopathic mouse models.

That said, it is important to note that we cannot presently rule out additional, later roles for HH signaling in laryngeal morphogenesis. On the contrary, specific ablation of *smoothened* in post-specification neural crest using *Wnt1*^{Cre} elicits a complete loss of the neural crest-derived thyroid cartilage (Jeong et al., 2004), though the effect of that manipulation on the vocal folds was not reported. Likewise, our deletion of *fuz* with *Wnt1*^{Cre} also caused disruption of thyroid cartilage morphology (Fig. S2), though this effect was less severe than that seen with smoothened disruption (Jeong et al., 2004).

Finally, *sonic hedgehog* is strongly expressed in the epithelial cells lining the glottis and the HH transducer *gli1* is expressed in the adjacent vocal folds in E11.5 mice (Lungova et al., 2015), suggesting another potential site of action. Future studies using conditional genetic approaches to assess the temporal and spatial requirements will be required before a comprehensive picture of HH signaling in the larynx can emerge.

Together, the data here provide new insights for future studies in two distinct areas. First, they shed light on the mechanisms of mammalian laryngeal development and suggest that the mouse larynx provides a tractable animal model for exploring the nexus between laryngeal structure and function. Second, they offer new insights into the role of neural crest in laryngeal morphogenesis, which may inform our understanding of the evolution of vocalization in vertebrates.

Embryonic origins of the mammalian larynx and vocal folds

Fate mapping is a critical prerequisite for understanding the etiology of defects in development, so our understanding of laryngeal development has been hindered by a lack of directed fate mapping of this organ. In fact, our knowledge of lineage relationships in the mouse larynx comes only from tangential findings in studies focused on other topics. The fate mapping data presented here therefore provides substantial insight and serves as a useful complement to the thorough fate maps of pharyngeal regions in birds and amphibians. We consider several notable findings:

First, our data demonstrate a mixed origin for laryngeal cartilages. Indeed, we find a mixed lineage even within a single cartilage element, with the thyroid cartilage being predominantly, but not completely, derived from *Wnt1-cre*-labeled neural crest descendants (Figure 3). Specifically, the caudal ventral midline of this cartilage was of mesodermal origin, labeled by *Mesp1-cre* (Figure 4). This result adds the thyroid cartilage to the roster of individual skeletal elements assembled by fusion of crest and mesoderm-derived mesenchymal precursors (e.g. (Le Lievre, 1978; Noden, 1988). In addition, we found no evidence for neural crest contribution to the arytenoid or cricoid cartilages, and instead our *Mesp1-cre* lineage data suggest a mesodermal origin for these elements (Figs. 3, 4).

These findings contradict a previous report suggesting a neural crest origin for all three laryngeal cartilages (thyroid, cricoid and arythenoid) with the anterior mesoderm boundary at the tracheal level (Matsuoka et al., 2005). However, several independent lines of evidence support our conclusion of distinct lineages for the laryngeal cartilages. First, we found no evidence for neural crest contribution to these cartilages using either *Wnt1* or *Pax3* promoters for lineage labeling. Second, conditional deletion of *Smoothened* or *Sox9* using *Wnt1-cre* results in specific loss of the thyroid cartilage but leaves the cricoid and arytenoids intact (Jeong et al., 2004; Mori-Akiyama et al., 2003). A third line of evidence comes from whole animal loss-of-function for *R-spondin2*, which functions as a modulator of Wnt signaling throughout development (de Lau et al., 2014). In both *R-spondin2* mutants and *Rspondin2/Lrp6* double mutants, both cricoid and arytenoid cartilages are absent, while the thyroid cartilage remains unaffected (Bell et al., 2008; Yamada et al., 2009). Because neural crest and mesoderm-derived craniofacial structures are known to respond differently to Wnt signaling (e.g. (Barrell et al. 2012, Li et al. 2015, Quarto et al. 2010), these data suggest distinct embryological origins for these cartilages. Fourth, our fate mapping data are consistent with avian fate maps in which the arytenoid and cricoid cartilages have a mesodermal origin, demonstrated both by transplantation and clonal analysis after retroviral labeling (Evans and Noden, 2006; Noden, 1986a). Finally, the amphibian pharyngeal skeleton, while considered to retain a more ancestral form, is nonetheless derived from a combination of neural crest and mesoderm (Sefton et al., 2015).

A second interesting finding concerns the cranial mesodermal origin for the vocal fold muscles (Figure 4). This finding is in contrast to what has been previously described; lineage analysis suggested a somitic origin of laryngeal muscles in both birds (Couly et al., 1992; Huang et al., 1997; Noden, 1983, 1986b) and amphibians (Piekarski and Olsson, 2007). Our combined $Pax3^{Cre}$ and $Isl1^{Cre}$ lineage data indicate that the mammalian vocal fold muscles are not of somitic origin but derived from cranial mesoderm, consistent with recent studies performed in mice (Gopalakrishnan et al., 2015; Lescroart et al., 2015).

Finally, the data argue for a neural crest origin for diverse connective tissues in the larynx, including the vocal ligaments and thyroglottal connective tissue (Figure 3). These

findings are significant because the viscoelastic properties of such connective tissues play an important role in sound production in mammals (see below).

Thus, our findings extend previous work highlighting the intricate interrelationship between migratory neural crest- and mesoderm-derived muscles during craniofacial morphogenesis (Noden and Trainor, 2005). Indeed, interactions between cranial mesoderm and cranial neural crest cells are essential for the normal patterning of the complex musculature of the head (Grenier et al., 2009; Heude et al., 2010; Rinon et al., 2007), perhaps explaining the lack of differentiated muscle in the crest-infused larynx of *Fuz* mutant mice (Figure 2). As such, our new data from the mammalian larynx complement existing work in other regions of the vertebrate head and highlight the key role of neural crest in the evolution of craniofacial morphology in general and the vocal apparatus specifically.

Excess neural crest as a common feature underlying craniofacial ciliopathies

Human ciliopathies commonly involve craniofacial defects as well as laryngeal and voice defects, including breathy voices in Bardet-Biedl Syndrome and a hoarse voice in Joubert and Oral-Facial-Digital Syndromes. Moreover, laryngeal stenosis or narrowing is observed in ciliopathies (Hayes et al., 2008; Silengo et al., 1987), consistent with glottic narrowing in *Gli3* mutants. Interestingly, Barnes Syndrome is a clinical entity that very closely overlaps the spectrum of defects in the known ciliopathy Jeune syndrome, but with the addition of severe laryngeal defects (Barnes et al., 1969; Burn et al., 1986). The genetic basis for Barnes syndrome is unknown, but it is possible that mutations in *Fuz* or its interacting CPLANE proteins may be involved (Toriyama et al., 2016).

In all cases, the embryological basis for human laryngeal defects remains only very poorly understood, but data here and elsewhere argue that excess neural crest may be a central causative agent. For example, the severely deranged *Fuz* larynx was found to be filled with *Wnt1-cre* labeled crest-derived mesenchymal cells (Figure 5), which we interpret as a more severe version of the defect observed in *Gli3* mutants. Likewise, the high arched palate that characterizes diverse ciliopathies is also present in *Fuz* mutant mice, where it is accompanied by an excess of neural crest (Tabler et al., 2013). Moreover, we have also recently described a novel skull defect in *Fuz* mutant mice in

549 which mesoderm derived parietal bones of the skull fail to form at the expense of
550 expanded neural crest-derived frontal bones (Tabler et al., 2016). Importantly, we also
551 find that a milder version of that phenotype is present in *gli3* mutant mice (Tabler et al.,
552 2016). We conclude then that laryngeal, palatal, and skull defects arising from defective
553 cilia-mediated Gli signaling share a common etiology rooted in excessive neural crest.
554
555 **Laryngeal developmental biology, neural crest, and the evolution of animal**
556 **vocalization.**
557
558 Our work here focuses on a tractable model organism with well-developed genetic tools
559 to explore the developmental biology of the mammalian larynx, revealing a key role for
560 neural crest. An important implication of the work, however, is that similar studies in non-
561 model animals could substantially advance our understanding of animal communication.
562
563 For example, the Panamanian tungara frog is a deeply studied model for evolution by
564 sexual selection (Ryan, 1985). The complex mating call of the tungara frog is generated
565 by a remarkable, sexually dimorphic elaboration of larynx called the fibrous mass
566 (Griddi-Papp et al., 2006). Strikingly, the embryonic origins of the fibrous mass and the
567 molecular genetic systems underlying its development are entirely unknown. However,
568 understanding its morphogenesis is important, as the final size and shape of the fibrous
569 mass differs between related species in the *Physaleamus* genus, as do the calls
570 produced by these species (Ryan, 1990).
571
572 Reptiles provide another interesting context for future study. While alligators have a
573 vocal folds relatively similar to that of mammals (Riede et al., 2015), snakes and
574 tortoises have highly derived larynges, in which novel vibrating structures take the place
575 of vocal folds. In bull snakes, defensive hissing sounds are generated by a flexible
576 horizontal shelf in the larynx (Young et al., 1995), while in tortoises, sound appears to be
577 generated by elastic bands on the lateral walls of the larynx (Sacchi et al., 2004). The
578 embryonic tissue origins of these structures, as well as the molecular controls that guide
579 their development, will be of interest.
580
581 In all three cases above, these laryngeal specializations are not muscular, but rather
582 resemble connective tissue. Our finding of a neural crest origin for connective tissue in

583 the mouse larynx suggests that novel vocalization structures in other animals may be
584 crest derived. In light of the importance of neural crest in the diversification of vertebrate
585 craniofacial structures (Frisdal and Trainor, 2014; Le Douarin and Dupin, 2012), we
586 propose that broader study of laryngeal developmental biology will shed light on the
587 evolutionary diversification of vertebrate vocalization mechanisms.
588
589 **Form and function in the mammalian larynx**
590
591 The ultrasonic calls of rodents have emerged as a useful model for studies of
592 mammalian vocalization (Arriaga et al., 2012; Fischer and Hammerschmidt, 2011)
593 (Heckman et al., 2016; Portfors and Perkel, 2014). Unlike the audible vocalizations
594 generated by vibrations due to the pressure differential across the apposed vocal folds,
595 rodent USVs are generated by a planar impinging air jet (Mahrt et al., 2016).
596 Nonetheless, USVs are generated by the larynx and vocal fold adduction is an important
597 factor both for sound production generally and for frequency modulation (Johnson et al.,
598 2010; Riede, 2013). Indeed, direct imaging during USV production revealed a tight
599 apposition of the vocal folds but an absence of vibrations normally observed during
600 audible vocalization (Sanders et al., 2001). Moreover, many physiological parameters of
601 mouse USV production parallel those of audible vocalization in other mammals (Riede,
602 2011, 2013). Because so little is known about the etiology of human laryngeal birth
603 defects and their relationship to voice dysfunction, we suggest that studies in mouse
604 models will be informative.
605
606 We focused on pup isolation vocalizations, which are acoustically distinct from -and
607 simpler than- adult ultrasonic vocalizations (Liu et al., 2003). Pup calls are also
608 processed preferentially in mothers (Elyada and Mizrahi, 2015; Liu and Schreiner, 2007)
609 and elicit maternal approach, retrieval and care (Sales and Pye, 1974). We found that
610 *Gli3*$^{xt/+}$ pups produce vocalizations with durations and average frequencies that are not
611 significantly different from those of their control littermates, however the bandwidth of
612 these vocalizations is significantly different. Moreover, our more fine-grained analysis of
613 vocalization shapes revealed that control and mutant mice differed in the proportion of
614 specific vocalization types produced. In particular, *Gli3*$^{xt/+}$ mutation decreased the
615 propensity of mice to make step vocalizations with abrupt frequency discontinuities, also

known as ‘punctuated’ (Panksepp et al., 2007) or ‘jump’ (Hanson and Hurley, 2012) syllables.

The mechanisms by which such step syllables are generated remain unclear, but we consider two possible explanations for this phenotype. First, vocalization requires exquisite neural control (Arriaga et al., 2012; Van Daele and Cassell, 2009), and HH signaling is known to control neural patterning (Briscoe and Therond, 2013). It may be, then, that alterations in neural pattern in these mice result in imperfect neural control of the larynx. However, our data on overall acoustic structure of calls in the mutant mice argue against this explanation. For example, call duration in rats, another rodent with similar ultrasonic vocalizations (Sales and Pye, 1974), is precisely correlated with EMG activity of laryngeal muscles, and the activity patterns of these muscles during mouse ultrasonic vocalization reflect patterns seen in other mammals during audible phonation (Riede, 2011, 2013). However, we found that duration of vocalizations was the same between control and mutant mice (Figure 8). In addition, disruption of the vocal center of the adult mouse cortex leads to changes in the distribution of mean frequencies of vocalizations (Arriaga et al., 2012), a parameter that was not affected in our *Gli3*$^{xt/+}$ mice (Figure 8). Conversely, manipulation of the vocal center did not alter the distribution of syllables produced (Arriaga et al., 2012), while *Gli3* mutation did (Figure 9). Finally, step vocalizations like those affected in our mutant mice are not correlated with either thyroarytenoid muscle EMG activity or sub-glottal pressure (Riede, 2011, 2013); and in fact, such step vocalizations can be produced independently of muscle or neural activity in excised bat larynges (Kobayasi et al., 2012).

These data suggest that such steps may result from a passive biomechanical effect in the larynx itself, leading us to prefer the alternative explanation that defective vocalization in *Gli3*$^{xt/+}$ mice results from defects in the larynx. By disrupting the normally tight connection of vocal fold muscles to the thyroid cartilage, we propose that the excess neural crest-derived connective tissue observed in the larynges of *Gli3*$^{xt/+}$ heterozygous mice may disrupt the biomechanics of the vocal folds and thereby impair normal sound production. Ultimately, further studies will be required to better define the source of vocalization defects in *Gli3* mutant mice. Importantly, however, the data here demonstrate that mouse models can both inform our understanding of mammalian

vocalization and could also provide insights into the etiology of human laryngeal and voice defects.

Materials and Methods

Mouse lines

The following mouse lines were used: *Gli3*$^{xt\text{-}J}$ (Hui and Joyner, 1993; Johnson, 1967); *Wnt1-cre*: *Tg:(Wnt1-cre)11Rth* (Danielian et al., 1998) (Danielian et al., 1998 PMID: 9636087); *Mesp1*^{Cre} (Saga et al., 1999); *Isl1*$^{Cre/+}$ (Srinivas et al., 2001) *Pax3*$^{Cre/+}$ (Engleka et al., 2005) and reporter line *R26*^{tdTomato} (Ai9; Madisen et al., 2010), *R26*$^{mT/mG}$: GT(Rosa)26Sortm4(ACTB-tdTomato-EGFP)Luo (Muzumdar et al., 2007), Fuz mutants: *Fuz*$^{gt(neo)}$ (Gray et al., 2009). Genotyping was performed as described in original publications. All animal work was performed in accordance with approved IACUC protocols at the University of Texas at Austin.

Histology and morphometrics

All immunohistochemistry, skeletal and histological staining were performed according to standard protocols. All embryos were collected in cold PBS and fixed in 4% paraformaldehyde. All embryos were sectioned horizontally at 18µm for cryosections and 4µm for paraffin sections. R26RmT/mG cryosections were stained with DAPI (1:1000) and then coverslipped with Vectashield (Vector Labs). Primary antibodiey used for immunohistochemistry on cryosections: anti-human Desmin (D33, Dako). Secondary antibodies used were Alexafluor 488 (Life Technologies) at 1:500. Hematoxylin and eosin staining and trichrome staining (HT25A, Sigma) were performed at the Dell Pediatric Research Institute Tissue Processing Core. Area and width of morphological features were determined in Fiji using the freehand selection and straight line tools, respectively. Two-four representative sections were measured from each biological replicate. All histological sections were imaged with a 20X lens on a Scanscope (Aperio, Leica) and processed via ImageScope (Aperio, Leica) and Adobe Photoshop.

Recording and extracting mouse vocalizations

Male *Gli3*$^{/xt/+}$ mice were mated with Swiss Webster females (Charles River Laboratories). 5 days post-natal pups were separated from the mother and isolated on

bedding in a recording chamber. Mouse vocalizations were recorded with an Ultrasoundgate 416H (Avisoft) sound recording system with a CM16/CMPA microphone (Avisoft) at a 250 kHz sampling rate and 16 bit resolution using Avisoft-RECORDER software, with the microphone suspended 5 cm from the pup. The start and stop times of ultrasonic vocalizations were automatically detected and frequency contours extracted using Ax (Seagraves et al., 2016; https://github.com/JaneliaSciComp/Ax). Briefly, time overlapped segments were Fourier transformed using multiple discrete prolate spheroidal sequences as windowing functions, followed by an F-test to identify time–frequency points with intensity significantly above noise ($P<0.01$). Acoustic segmentation was verified, and, if necessary, corrected manually. Signals that had exceeded the amplitude limit of the recording system (had “clipped”) were excluded from analysis.

Generating map of vocal repertoire space

In order to compare the vocalizations of the two genotypes we create a single high-dimensional space that fully captures all the acoustic structure in the frequency contours. We then visualize that high dimensional space using dimensionality reduction to create a two-dimensional map of the vocal repertoire. In this way we are able to look at vocal similarity across the vocal repertoire in the same reference frame for both genotypes. Frequency contours were mean frequency subtracted, and then all pairs of frequency contours were compared using dynamic time warping (Sakoe and Chiba, 1978) to create an all-to-all distance matrix ((9013x9013)/2 comparisons). The data in this high dimensional distance matrix was then embedded into two dimensions using t-SNE (van der Maaten and Hinton, 2008) (transition entropy=5, relative convergence of cost function to 0.0001). t-Distributed Stochastic Neighbor embedding (t-SNE) is a nonlinear embedding method that aims to preserve local structure within a data set. This is achieved through placing points into a low-dimensional space such that points that were nearby in a higher-dimensional representation remain nearby in the new representation. Specifically, this embedding is calculated through optimally matching local similarity measures obtained in both the high and low dimensional spaces. Unlike other non-linear embedding approaches, this technique preserves clusters within a data set, but will allow for larger length scale distortions in order to obtain the desired dimensionality reduction. This is precisely the opposite of PCA, multi-dimensional scaling, or Isomap (Tenenbaum et al., 2000), which aim to preserve global structure at the expense of local distortions. Because t-SNE preserves local neighbor relationships from the full-

719 dimensional space of the frequency contour, regions in the map can be thought of as
720 rough categories of vocalizations based on acoustic similarity. However, only local
721 relationships are preserved, long-length-scale relationships are distorted, which means
722 that the axes of the map are inherently arbitrary. A detailed description of applying t-
723 SNE to a behavioral data set can be found in (Berman et al., 2014).
724
725 **Acoustic analyses**
726 Simple measures of acoustic structure (duration, bandwidth, and average frequency
727 were calculated from the automatically extracted contours). Differences between WT
728 and HT in these simple measures were tested using single factor ANOVAs on average
729 values for each individual. To test for differences in the number of step and non-step
730 vocalizations between WT and HT each vocalization was labeled as a step or non-step
731 based on their position in the vocal repertoire map. This labeling was automatic and
732 blind to genotype. Regions of significant difference between the HT and WT maps were
733 determined using bootstrapping, where we estimated the variation in the measured
734 probability density functions due having a finite number of vocalizations in the data set.
735 This was achieved through separately resampling the 2-D embeddings of the
736 vocalizations for each case (WT and HT) with replacement 10,000 times and convolving
737 each of these resampled data sets with a Gaussian of width 4 to create distributions,
738 $q_{HT}(\rho|x,y)$ and $q_{WT}(\rho|x,y)$ for each of the PDFs at every point in space ($q_{HT}(\rho|x,y) \equiv$
739 $Prob(\rho_{HT}(x,y)=\rho)$ and $q_{WT}(\rho|x,y) \equiv Prob(\rho_{WT}(x,y)=\rho)$. These spatially-varying
740 PDFs were obtained by fitting a Gaussian mixture model to the sampled PDFs (up to
741 three peaks, chosen at each point by maximizing the Akaike Information Criterion). As
742 we assume that the two populations are sampled independently, the probability that
743 $\rho_{HT}(x,y)$ is greater than $\rho_{HT}(x,y)$, defined here as $P_{HT}(x,y)$, is thus given by numerically
744 integrating $P_{HT}(x,y) = \int_0^\infty \int_0^{\rho\_HT} q_{WT}(\rho_{WT}|x,y) q_{HT}(\rho_{HT}|x,y) d\rho_{WT}\, d\rho_{HT}$. Regions of
745 significant difference are those where $P_{HT}(x,y) < \alpha$ or $P_{HT}(x,y) > 1-\alpha$. Here, we used
746 $\alpha = .05$, but corrected for multiple comparisons using the Šidák correction. We
747 conservatively assume the number of comparisons to be $2\text{^}H$, where H is the entropy of
748 the original 2D embedding of our data set ($H = -\int\int \rho(x,y) log_2\, \rho(x,y) dx\, dy$, where
749 $\rho(x,y) = \frac{1}{2}(\rho_{HT}(x,y) + \rho_{WT}(x,y))$). To test for differences in the number of step and
750 non-step vocalizations between WT and HT each vocalization was labeled as a step or
751 non-step based on their position in the vocal repertoire map (see Figure 9C,

752 vocalizations in green regions were labeled step, vocalizations in the pink region were
753 labeled non-step). Because the map was generated using vocalizations from both
754 genotypes, this labeling was automatic and blind to genotype. We then compared the
755 number of step and non-step vocalizations in the two genotypes using the χ^2 test.
756
757 **Acknowledgements:**
758
759 We thank D. Parichy and T. Arlson for critical reading. This work was supported by an
760 NRSA to J.T. from the NIDCR (F32DE023272); funding to S.T. from the Institut Pasteur,
761 Association Française contre le Myopathies, and Agence Nationale de la Recherche
762 (Laboratoire d'Excellence Revive, Investissement d'Avenir; ANR-10-LABX-73); and NIH
763 R01HD073151 to S.A.V. and R01HD085901 to J.B.W. SERE is supported by the
764 Howard Hughes Medical Institute; JBW was once an early career scientist of the HHMI.
765
766
767 **Figure Legends:**
768
769 **Figure 1. Anatomy of the mouse larynx.** (A) Diagram representing ventral view of
770 mouse laryngeal anatomy. Dashed lines indicate sectional plane represented in panels
771 C-F. (B) Ventral view of an excised adult larynx stained with alcian blue marking
772 cartilage. (C-E) H&E staining of horizontal sections of E18.5 mouse larynx. Sectional
773 plane is indicated in A. Diagrams indicate anatomy observed in sections. (F) H&E
774 staining of sagittal section of E18.5 mouse larynx. Diagram indicates anatomy
775 represented in section. Scale bar indicates 500μm. Abbreviations: (AC) Arytenoid
776 Cartilage, (CC) Cricoid Cartilage, (CT) Cricothyroid muscle, (E) Esophagus, (G) Glottis,
777 (L) Larynx, (LCA) Lateral Cricoarytenoid muscle, (PCA) Posterior Cricoarytenoid muscle,
778 (T) Tongue, (TAM) Thyroarytenoid Muscle, (TC) Thryoid Cartilage, (TgCT) Thyroglottal
779 connective tissue, (Tr) Trachea, (VL) Vocal Ligament, (VM) Vocalis Muscle, (VF) Vocal
780 fold. (V) and (D) indicate dorso-ventral axes.
781
782 **Figure 2. Laryngeal anatomy is disrupted in *Fuz* and *Gli3* mutants.** (A-C) H&E
783 staining of horizontal sections of E18.5 larynges. (A'-C') Diagrams of anatomy shown in
784 (A-C). *Fuz* mutant larynges (B-B') are significantly altered compared to controls, (A-A').
785 Connective tissue in mutants (light green, C') is increased in mutants compared to

controls (A-A'), while cartilage and muscle are irregularly patterned. *Gli3*$^{-/-}$ larynges are less altered than *Fuz*$^{-/-}$ embryos compared to controls (A-A'). Thyroglottal Connective tissue appears increased in *Gli3* mutants (light green, red arrow, C'). Scale bars indicates 500μm. Abbreviations: (AC) Arytenoid Cartilage, (CC) Cricoid Cartilage, (CT) Cricothyroid muscle, (G) Glottis, (L) Larynx, (LCA) Lateral Cricoarytenoid muscle, (PCA) Posterior Cricoarytenoid muscle, (T) Tongue, (TAM) Thyroarytenoid Muscle, (TC) Thryoid Cartilage, (TgCT) Thyroglottal connective tissue, (Tr) Trachea, (VL) Vocal Ligament, (VM) Vocalis Muscle, (VF) Vocal fold. (V) and (D) indicate dorso-ventral axes.

Figure 3. Thyroid cartilage and vocal ligament are mostly neural crest derived. (A) Diagram representing anatomy in (B-B'). (B-B') Horizontal section of rostral E18.5 *Wnt1*$^{Cre/+}$*; R26*^{mTmG} larynx. Neural crest derivatives are labeled in green while other tissues are labeled with Magenta. (B-C) Scale bar indicates 200 μm. (C) Diagram representing anatomy in (D-D') Horizontal section of caudal E18.5 *Wnt1*$^{Cre/+}$*; R26*^{mTmG} larynx. (E) Diagram representing anatomy in (F-F'). (F-F') Horizontal caudal section of E18.5 *Pax3*$^{Cre/+}$*; R26*^{tomato} larynx that is also immunostained for Desmin which marks muscle (Green and yellow in cells that have also expressed *Pax3*) and nuclei (Blue). (G) Diagram representing anatomy in (H-H'). (H-H') Sagittal section of E18.5 *Wnt1*$^{Cre/+}$*; R26*^{mTmG} larynx. Thyroglottal Insets are indicated with white dotted box. (F-F') Scale bars indicates 100μm. Abbreviations: (AC) Arytenoid Cartilage, (CC) Cricoid Cartilage, (CT) Cricothyroid muscle, (E) Esophagus, (G) Glottis, (L) Larynx, (LCA) Lateral Cricoarytenoid muscle, (PCA) Posterior Cricoarytenoid muscle, (TAM) Thyroarytenoid Muscle, (TC) Thryoid Cartilage, (TgCT) Thyroglottal connective tissue, (Tr) Trachea, (VL) Vocal Ligament, (VM) Vocalis Muscle, (VF) Vocal fold. (V) and (D) indicate dorso-ventral axes..

Figure 4. Vocal fold muscles are from cranial mesodermal origin (A) Horizontal section of rostral E18.5 *Mesp1*^{Cre}*; R26*^{Tomato} larynx showing that the arytenoid and cricoid cartilages, and Desmin-positive vocal fold muscles are derived from mesoderm. (B) Horizontal section of rostral E18.5 *Islet1*^{Cre}*; R26*^{mTmG} larynx indicating that all the vocal fold muscles are of cranial mesoderm origin. (C) Horizontal section of E18.5 larynx of *Mesp1*^{Cre}*; R26*^{mTmG} mouse showing the ventral part of the thyroid cartilage derived from mesoderm. (D) Diagram of anatomy represented in (A-C). The mesoderm derivatives are labeled in light green while the specific muscular cranial mesoderm derivatives are

labeled in dark green. Scale bars indicates 100μm. Abbreviations: (AC) Arytenoid Cartilage, (CC) Cricoid Cartilage, (CT) Cricothyroid muscle, (LCA) Lateral Cricoarytenoid muscle, (PCA) Posterior Cricoarytenoid muscle, (TAM) Thyroarytenoid Muscle, (TC) Thryoid Cartilage, (Tr) Trachea, , (VM) Vocalis Muscle, (VF) Vocal fold.

Figure 5. Neural crest is expanded in *Fuz* and *Gli3* mutant larynges. (A-C) Horizontal section of E14.25 larynges. (A) Wild Type *Wnt1^{Cre}::mGFP* labeled larynx (B) *Fuz$^{-/-}$; Wnt1$^{Cre/+}$; R26^{mTmG}* larynx. (C) *Gli3$^{-/-}$;Wnt1$^{Cre/+}$; R26^{mTmG}*. Neural crest is labeled in green and other tissues in magenta. (A'-C') Diagrams representing anatomy found in (A-C). Abbreviations: (AC) Arytenoid Cartilage, (CC) Cricoid Cartilage, (CT) Cricothyroid, (E) Esophagus, (G) Glottis, (L) Larynx, (LCA) Lateral Cricoarytenoid, (PCA) Posterior Cricoarytenoid muscle, (TAM) Thyroarytenoid Muscle, (TC) Thryoid Cartilage, (T) Tongue, (Tr) Trachea, (VL) Vocal Ligament, (VM) Vocalis Muscle, (VF) Vocal fold. (V) and (D) indicate dorsal ventral axes.Scale bars indicates 200μm.

Figure 6. Expanded Thyroglottal connective tissue in *Gli3* mutants is neural crest derived. (A-C) Horizontal sections of E18.5 ventral larynx in *Gli3$^{+/+}$;Wnt1$^{Cre/+}$; R26^{mTmG}* (A) *Gli3$^{+/-}$;Wnt1$^{Cre/+}$; R26^{mTmG}* (B) *Gli3$^{-/-}$;Wnt1$^{Cre/+}$; R26^{mTmG}* (C) embryos. (A'-C') Diagrams representing anatomy observed in (A-C). Black dotted line indicates sectional plane for (D-F'). (D-F) H&E staining of midline sagittal sections of E18.5 larynges in *Gli3$^{+/+}$* (D), *Gli3$^{+/-}$* (E); *Gli3$^{-/-}$* (F) embryos. (D'-E') Magnified view of Thyroglottal Connective tissue (green arrows) of the vocal pouch from sections in (D-F). Abbreviations: (E) Esophagus, (G) Glottis, (VL) Vocal Ligament, (VM) Vocalis Muscle, (TAM) Thyroarytenoid Muscle. Scale bars indicates 100μm.

Figure 7. *Gli3* mutant laryngeal morphology is significantly altered. (A) Diagram representing laryngeal measurement presented in (B-F). (B) Quantification of total laryngeal cross sectional area excluding extrinsic muscles in E18.5 *Gli3$^{+/+}$* (*n*=5), *Gli3$^{+/-}$* (*n*=5), *Gli3$^{-/-}$* (*n*=5) embryos (orange, A). (C) Quantification of Vocal ligament area E18.5 *Gli3$^{+/+}$*, *Gli3$^{+/-}$*, *Gli3$^{-/-}$* embryos (blue, A). (D) Quantification of vocal fold muscle area in E18.5 *Gli3$^{+/+}$*, *Gli3$^{+/-}$*, *Gli3$^{-/-}$* embryos. (E) Quantification of Thyroglottal connective tissue are in E18.5 *Gli3$^{+/+}$*, *Gli3$^{+/-}$*, *Gli3$^{-/-}$* embryos. (F) Quantification of Glottic space in E18.5 *Gli3$^{+/+}$*, *Gli3$^{+/-}$*, *Gli3$^{-/-}$* embryos. P values, * = 0.05, ** =0.01, ***>0.001, **** >0.0001.

Figure 8. WT and HT vocalizations do not differ on simple acoustic measures
(A) Examples of *Gli3*$^{+/-}$ vocalizations with (top panel) and without (bottom panel) frequency steps. (B) Examples of *Gli3*$^{+/-}$ vocalizations with (top panel) and without (bottom panel) frequency steps. (C) Duration of *Gli3*$^{+/-}$ (blue) and *Gli3*$^{+/-}$ (red) pup vocalizations. Average values for each individual (left panel) and summary histogram of all vocalizations (right panel). (D) Bandwidth of *Gli3*$^{+/+}$ (blue) and *Gli3*$^{+/-}$ (red) pup vocalizations. Average values for each individual (left panel) and summary histogram of all vocalizations (right panel). (E) Mean frequency of *Gli3*$^{+/-}$ (blue) and *Gli3*$^{+/-}$ (red) pup vocalizations. Average values for each individual (left panel) and summary histogram of all vocalizations (right panel).

Figure 9: Map of pup vocal repertoire reveals differences in acoustic structure
(A) Position of each vocalization within the vocal repertoire map (Individual vocalizations). To generate the map, we defined the difference between two vocalizations to be the dynamically time-warped (Sakoe & Chiba, 1978) mean squared error between them. Low-dimensional structure is then extracted from these distances using t-Distributed Stochastic Neighbor Embedding (t-SNE) [van der Maaten (2008) & Berman (2014)], resulting in the points seen in (A). This embedding results in a clustered structure, This two dimensional non-linear embedding preserves local neighbor relationships in the original high dimensional space. Because this embedding could be equivalently presented at any angle, the vertical and horizontal axes here are arbitrarily chosen and do not represent, for example, the leading directions of variation within the data set. (B) Estimated density of the vocalizations within the map (total vocalization density map). (C) Overlapped frequency contours for regions across the vocal repertoire map, showing the distribution of syllable types (Frequency Contour Distribution). (D) *Gli3*$^{+/+}$ vocalizations in the map. (E) *Gli3*$^{+/-}$ vocalizations in the map. (F) Difference between the maps with significance regions outlined. ($F_{1,9}$=0.04, p=0.85) were observed, and only non-significant changes we observed in frequency bandwidth ($F_{1,9}$=1.26, p=0.29) and average frequency ($F_{1,9}$=0.28, p=0.61)

Figure 2-Figure Supplemental 1. Fgf8 reduction in Fuz mutants partially rescues laryngeal phenotypes.
(A) Diagram indicating sectional plane of E16.5 embryos. (B-C) Trichrome staining of frontal E16.5 *Fuz*$^{+/+;}$ *Fgf8*$^{Lacz/+}$ (B), *Fuz*$^{+/+}$(C), and *Fuz*$^{-/-;}$ *Fgf8*$^{Lacz/+}$ embryos. (B'-C')

888 Diagrams illustrating anatomy observed in (B-C). Hyoid bone (dark blue), thyroid (light
889 blue), arytenoid (purple) and cricoid cartilages are present in *Fuz*$^{+/+;}$ *Fgf8*$^{Lacz/+}$ and *Fuz*$^{-/-;}$
890 *Fgf8*$^{Lacz/+}$ embryos.
891
892 ***Figure 2-Figure Supplemental 2.***
893 (A-B) H&E staining of horizontal sections E16.5 larynges in *Fuz*$^{Fl/+;}$ *Wnt1*$^{Cre/+}$ (A) and
894 *Fuz*$^{Fl/+;}$ *Wnt1*$^{Cre/+}$ (B) embryos.
895
896 **References:**
897
898 Aoto, K., Nishimura, T., Eto, K., and Motoyama, J. (2002). Mouse GLI3 regulates Fgf8
899 expression and apoptosis in the developing neural tube, face, and limb bud. Dev Biol
900 *251*, 320-332.
901 Aronson, A.E., and Bless, D.M. (2009). Clinical Voice disorders (New York: Thieme
902 Medical Publishers).
903 Arriaga, G., Zhou, E.P., and Jarvis, E.D. (2012). Of mice, birds, and men: the mouse
904 ultrasonic song system has some features similar to humans and song-learning birds.
905 PLoS ONE *7*, e46610.
906 Barnes, N.D., Hull, D., and Symons, J.S. (1969). Thoracic dystrophy. Arch Dis Child *44*,
907 11-17.
908 Beales, P.L., Elcioglu, N., Woolf, A.S., Parker, D., and Flinter, F.A. (1999). New criteria
909 for improved diagnosis of Bardet-Biedl syndrome: results of a population survey. J Med
910 Genet *36*, 437-446.
911 Bell, S.M., Schreiner, C.M., Wert, S.E., Mucenski, M.L., Scott, W.J., and Whitsett, J.A.
912 (2008). R-spondin 2 is required for normal laryngeal-tracheal, lung and limb
913 morphogenesis. Development *135*, 1049-1058.
914 Berman, G.J., Choi, D.M., Bialek, W., and Shaevitz, J.W. (2014). Mapping the
915 stereotyped behaviour of freely moving fruit flies. J R Soc Interface *11*.
916 Bose, J., Grotewold, L., and Ruther, U. (2002). Pallister-Hall syndrome phenotype in
917 mice mutant for Gli3. Hum Mol Genet *11*, 1129-1135.
918 Briscoe, J., and Therond, P.P. (2013). The mechanisms of Hedgehog signalling and its
919 roles in development and disease. Nat Rev Mol Cell Biol *14*, 416-429.
920 Burn, J., Hall, C., Marsden, D., and Matthew, D.J. (1986). Autosomal dominant
921 thoracolaryngopelvic dysplasia: Barnes syndrome. J Med Genet *23*, 345-349.
922 Carron, J.D. (2006). Bifid Epiglottis Revisited. Int J Pediatr Otorhinolaryngol *1*, 115-118.
923 Chai, Y., Jiang, X., Ito, Y., Bringas, P., Jr., Han, J., Rowitch, D.H., Soriano, P.,
924 McMahon, A.P., and Sucov, H.M. (2000). Fate of the mammalian cranial neural crest
925 during tooth and mandibular morphogenesis. Development *127*, 1671-1679.
926 Cohen, M.M. (2004). SHH and Holoprosencephaly. In Inborn Errors of Development,
927 C.J. Epstein, R.P. Erickson, and A. Wynshaw-Boris, eds. (New York: Oxford University
928 Press).
929 Collier, S., and Gubb, D. (1997). Drosophila tissue polarity requires the cell-autonomous
930 activity of the fuzzy gene, which encodes a novel transmembrane protein. Development
931 *124*, 4029-4037.
932 Couly, G.F., Coltey, P.M., and Le Douarin, N.M. (1992). The developmental fate of the
933 cephalic mesoderm in quail-chick chimeras. Development *114*, 1-15.

Creuzet, S., Schuler, B., Couly, G., and Le Douarin, N.M. (2004). Reciprocal relationships between Fgf8 and neural crest cells in facial and forebrain development. Proc Natl Acad Sci U S A *101*, 4843-4847.
Danielian, P.S., Muccino, D., Rowitch, D.H., Michael, S.K., and McMahon, A.P. (1998). Modification of gene activity in mouse embryos in utero by a tamoxifen-inducible form of Cre recombinase. Curr Biol *8*, 1323-1326.
de Lau, W., Peng, W.C., Gros, P., and Clevers, H. (2014). The R-spondin/Lgr5/Rnf43 module: regulator of Wnt signal strength. Genes Dev *28*, 305-316.
Eckel, H.E., and Sittel, C. (1995). Morphometry of the larynx in horizontal sections. Am J Otolaryngol *16*, 40-48.
Elyada, Y.M., and Mizrahi, A. (2015). Becoming a mother - circuit plasticity underlying maternal behavior. Curr Opin Neurobiol *35*, 49-56.
Evans, D.J., and Noden, D.M. (2006). Spatial relations between avian craniofacial neural crest and paraxial mesoderm cells. Dev Dyn *235*, 1310-1325.
Fischer, J., and Hammerschmidt, K. (2011). Ultrasonic vocalizations in mouse models for speech and socio-cognitive disorders: insights into the evolution of vocal communication. Genes Brain Behav *10*, 17-27.
Franca, M.M., Jorge, A.A., Carvalho, L.R., Costalonga, E.F., Vasques, G.A., Leite, C.C., Mendonca, B.B., and Arnhold, I.J. (2010). Novel heterozygous nonsense GLI2 mutations in patients with hypopituitarism and ectopic posterior pituitary lobe without holoprosencephaly. J Clin Endocrinol Metab *95*, E384-391.
Frisdal, A., and Trainor, P.A. (2014). Development and evolution of the pharyngeal apparatus. Wiley Interdiscip Rev Dev Biol *3*, 403-418.
Garstecki, D.C., Borton, T.E., Stark, E.W., and Kennedy, B.T. (1972). Speech, language, and hearing problems in the Laurence-Moon-Biedl syndrome. J Speech Hear Disord *37*, 407-413.
Goetz, S.C., and Anderson, K.V. (2010). The primary cilium: a signalling centre during vertebrate development. Nat Rev Genet *11*, 331-344.
Gopalakrishnan, S., Comai, G., Sambasivan, R., Francou, A., Kelly, R.G., and Tajbakhsh, S. (2015). A Cranial Mesoderm Origin for Esophagus Striated Muscles. Dev Cell *34*, 694-704.
Gray, R.S., Abitua, P.B., Wlodarczyk, B.J., Szabo-Rogers, H.L., Blanchard, O., Lee, I., Weiss, G.S., Liu, K.J., Marcotte, E.M., Wallingford, J.B.*, et al.* (2009). The planar cell polarity effector Fuz is essential for targeted membrane trafficking, ciliogenesis and mouse embryonic development. Nat Cell Biol *11*, 1225-1232.
Grenier, J., Teillet, M.A., Grifone, R., Kelly, R.G., and Duprez, D. (2009). Relationship between neural crest cells and cranial mesoderm during head muscle development. PLoS ONE *4*, e4381.
Griddi-Papp, M., Rand, A.S., and Ryan, M.J. (2006). Complex call production in túngara frogs. Nature *441*, 38.
Hall, J.G., Pallister, P.D., Clarren, S.K., Beckwith, J.B., Wiglesworth, F.W., Fraser, F.C., Cho, S., Benke, P.J., and Reed, S.D. (1980). Congenital hypothalamic hamartoblastoma, hypopituitarism, imperforate anus and postaxial polydactyly--a new syndrome? Part I: clinical, causal, and pathogenetic considerations. Am J Med Genet *7*, 47-74.
Hanson, J.L., and Hurley, L.M. (2012). Female Presence and Estrous State Influence Mouse Ultrasonic Courtship Vocalizations. PLoS ONE *7*.
Harel, I., Nathan, E., Tirosh-Finkel, L., Zigdon, H., Guimaraes-Camboa, N., Evans, S.M., and Tzahor, E. (2009). Distinct origins and genetic programs of head muscle satellite cells. Dev Cell *16*, 822-832.

Harrison, D.F.N. (1995). The anatomy and physiology of the mammalian larynx (Cambridge: Cambridge Univ. Press).
Haycraft, C.J., Banizs, B., Aydin-Son, Y., Zhang, Q., Michaud, E.J., and Yoder, B.K. (2005). Gli2 and Gli3 localize to cilia and require the intraflagellar transport protein polaris for processing and function. PLoS Genet *1*, e53.
Hayes, L.L., Simoneaux, S.F., Palasis, S., and Niyazov, D.M. (2008). Laryngeal and tracheal anomalies in an infant with oral-facial-digital syndrome type VI (Varadi-Papp): report of a transitional type. Pediatr Radiol *38*, 994-998.
Heckman, J., McGuinness, B., Celikel, T., and Englitz, B. (2016). Determinants of the mouse ultrasonic vocal structure and repertoire. Neurosci Biobehav Rev *65*, 313-325.
Henick, D.H. (1993). Three-dimensional analysis of murine laryngeal development. Ann Otol Rhinol Laryngol Suppl *159*, 3-24.
Heude, E., Bouhali, K., Kurihara, Y., Kurihara, H., Couly, G., Janvier, P., and Levi, G. (2010). Jaw muscularization requires Dlx expression by cranial neural crest cells. Proc Natl Acad Sci U S A *107*, 11441-11446.
Heydeck, W., and Liu, A. (2011). PCP effector proteins inturned and fuzzy play nonredundant roles in the patterning but not convergent extension of mammalian neural tube. Dev Dyn *240*, 1938-1948.
Heydeck, W., Zeng, H., and Liu, A. (2009). Planar cell polarity effector gene Fuzzy regulates cilia formation and Hedgehog signal transduction in mouse. Dev Dyn *238*, 3035-3042.
Hildebrandt, F., Benzing, T., and Katsanis, N. (2011). Ciliopathies. N Engl J Med *364*, 1533-1543.
Holy, T.E., and Guo, Z.S. (2005). Ultrasonic songs of male mice. Plos Biology *3*, 2177-2186.
Huang, R., Zhi, Q., Ordahl, C.P., and Christ, B. (1997). The fate of the first avian somite. Anat Embryol (Berl) *195*, 435-449.
Hui, C.C., and Joyner, A.L. (1993). A mouse model of greig cephalopolysyndactyly syndrome: the extra-toesJ mutation contains an intragenic deletion of the Gli3 gene. Nat Genet *3*, 241-246.
Ilagan, R., Abu-Issa, R., Brown, D., Yang, Y.P., Jiao, K., Schwartz, R.J., Klingensmith, J., and Meyers, E.N. (2006). Fgf8 is required for anterior heart field development. Development *133*, 2435-2445.
Jeong, J., Mao, J., Tenzen, T., Kottmann, A.H., and McMahon, A.P. (2004). Hedgehog signaling in the neural crest cells regulates the patterning and growth of facial primordia. Genes Dev *18*, 937-951.
Johnson, A.M., Ciucci, M.R., Russell, J.A., Hammer, M.J., and Connor, N.P. (2010). Ultrasonic output from the excised rat larynx. J Acoust Soc Am *128*, EL75-79.
Johnson, D.R. (1967). Extra-toes: anew mutant gene causing multiple abnormalities in the mouse. J Embryol Exp Morphol *17*, 543-581.
Jongmans, M.C., Admiraal, R.J., van der Donk, K.P., Vissers, L.E., Baas, A.F., Kapusta, L., van Hagen, J.M., Donnai, D., de Ravel, T.J., Veltman, J.A.*, et al.* (2006). CHARGE syndrome: the phenotypic spectrum of mutations in the CHD7 gene. J Med Genet *43*, 306-314.
Kaufman, M.H. (1992). The Atlas of Mouse Development (Academic Press).
Kobayasi, K.I., Hage, S.R., Berquist, S., Feng, J., Zhang, S.Y., and Metzner, W. (2012). Behavioural and neurobiological implications of linear and non-linear features in larynx phonations of horseshoe bats. Nature Communications *3*.
Le Douarin, N.M., and Dupin, E. (2012). The neural crest in vertebrate evolution. Curr Opin Genet Dev *22*, 381-389.

1034 Le Lievre, C.S. (1978). Participation of neural crest-derived cells in the genesis of the
1035 skull in birds. J Embryol Exp Morphol *47*, 17-37.
1036 Lescroart, F., Hamou, W., Francou, A., Theveniau-Ruissy, M., Kelly, R.G., and
1037 Buckingham, M. (2015). Clonal analysis reveals a common origin between nonsomite-
1038 derived neck muscles and heart myocardium. Proc Natl Acad Sci U S A *112*, 1446-1451.
1039 Li, J., Chen, F., and Epstein, J.A. (2000). Neural crest expression of Cre recombinase
1040 directed by the proximal Pax3 promoter in transgenic mice. Genesis *26*, 162-164.
1041 Liu, R.C., Miller, K.D., Merzenich, M.M., and Schreiner, C.E. (2003). Acoustic variability
1042 and distinguishability among mouse ultrasound vocalizations. J Acoust Soc Am *114*,
1043 3412-3422.
1044 Liu, R.C., and Schreiner, C.E. (2007). Auditory cortical detection and discrimination
1045 correlates with communicative significance. PLoS Biol *5*, e173.
1046 Lungova, V., Verheyden, J.M., Herriges, J., Sun, X., and Thibeault, S.L. (2015).
1047 Ontogeny of the mouse vocal fold epithelium. Dev Biol *399*, 263-282.
1048 Mahrt, E., Agarwal, A., Perkel, D., Portfors, C., and Elemans, C.P. (2016). Mice produce
1049 ultrasonic vocalizations by intra-laryngeal planar impinging jets. Curr Biol *26*, R880-
1050 R881.
1051 Maria, B.L., Boltshauser, E., Palmer, S.C., and Tran, T.X. (1999). Clinical features and
1052 revised diagnostic criteria in Joubert syndrome. J Child Neurol *14*, 583-590; discussion
1053 590-581.
1054 Matsuoka, T., Ahlberg, P.E., Kessaris, N., Iannarelli, P., Dennehy, U., Richardson, W.D.,
1055 McMahon, A.P., and Koentges, G. (2005). Neural crest origins of the neck and shoulder.
1056 Nature *436*, 347-355.
1057 Mori-Akiyama, Y., Akiyama, H., Rowitch, D.H., and de Crombrugghe, B. (2003). Sox9 is
1058 required for determination of the chondrogenic cell lineage in the cranial neural crest.
1059 Proc Natl Acad Sci U S A *100*, 9360-9365.
1060 Muzumdar, M.D., Tasic, B., Miyamichi, K., Li, L., and Luo, L. (2007). A global double-
1061 fluorescent Cre reporter mouse. Genesis *45*, 593-605.
1062 Nathan, E., Monovich, A., Tirosh-Finkel, L., Harrelson, Z., Rousso, T., Rinon, A., Harel,
1063 I., Evans, S.M., and Tzahor, E. (2008). The contribution of Islet1-expressing splanchnic
1064 mesoderm cells to distinct branchiomeric muscles reveals significant heterogeneity in
1065 head muscle development. Development *135*, 647-657.
1066 Neunuebel, J.P., Taylor, A.L., Arthur, B.J., and Egnor, S.E.R. (2015). Female mice
1067 ultrasonically interact with males during courtship displays. Elife *4*.
1068 Noden, D.M. (1983). The embryonic origins of avian cephalic and cervical muscles and
1069 associated connective tissues. Am J Anat *168*, 257-276.
1070 Noden, D.M. (1986a). Origins and patterning of craniofacial mesenchymal tissues. J
1071 Craniofac Genet Dev Biol Suppl *2*, 15-31.
1072 Noden, D.M. (1986b). Patterning of avian craniofacial muscles. Dev Biol *116*, 347-356.
1073 Noden, D.M. (1988). Interactions and fates of avian craniofacial mesenchyme.
1074 Development *103 Suppl*, 121-140.
1075 Noden, D.M., and Trainor, P.A. (2005). Relations and interactions between cranial
1076 mesoderm and neural crest populations. J Anat *207*, 575-601.
1077 Noirot, E. (1966). Ultra-Sounds in Young Rodents .I. Changes with Age in Albino Mice.
1078 Anim Behav *14*, 459-&.
1079 Ondrey, F., Griffith, A., Van Waes, C., Rudy, S., Peters, K., McCullagh, L., and
1080 Biesecker, L.G. (2000). Asymptomatic laryngeal malformations are common in patients
1081 with Pallister-Hall syndrome. Am J Med Genet *94*, 64-67.
1082 Panksepp, J.B., Jochman, K.A., Kim, J.U., Koy, J.J., Wilson, E.D., Chen, Q.L., Wilson,
1083 C.R., and Lahvis, G.P. (2007). Affiliative Behavior, Ultrasonic Communication and Social
1084 Reward Are Influenced by Genetic Variation in Adolescent Mice. PLoS ONE *2*.

1085 Park, T.J., Haigo, S.L., and Wallingford, J.B. (2006). Ciliogenesis defects in embryos
1086 lacking inturned or fuzzy function are associated with failure of planar cell polarity and
1087 Hedgehog signaling. Nat Genet *38*, 303-311.
1088 Piekarski, N., and Olsson, L. (2007). Muscular derivatives of the cranialmost somites
1089 revealed by long-term fate mapping in the Mexican axolotl (Ambystoma mexicanum).
1090 Evol Dev *9*, 566-578.
1091 Portfors, C.V., and Perkel, D.J. (2014). The role of ultrasonic vocalizations in mouse
1092 communication. Curr Opin Neurobiol *28*, 115-120.
1093 Putoux, A., Nampoothiri, S., Laurent, N., Cormier-Daire, V., Beales, P.L., Schinzel, A.,
1094 Bartholdi, D., Alby, C., Thomas, S., Elkhartoufi, N.*, et al.* (2012). Novel KIF7 mutations
1095 extend the phenotypic spectrum of acrocallosal syndrome. J Med Genet *49*, 713-720.
1096 Riede, T. (2011). Subglottal pressure, tracheal airflow, and intrinsic laryngeal muscle
1097 activity during rat ultrasound vocalization. J Neurophysiol *106*, 2580-2592.
1098 Riede, T. (2013). Stereotypic laryngeal and respiratory motor patterns generate different
1099 call types in rat ultrasound vocalization. J Exp Zool A Ecol Genet Physiol *319*, 213-224.
1100 Riede, T., Li, Z., Tokuda, I.T., and Farmer, C.G. (2015). Functional morphology of the
1101 Alligator mississippiensis larynx with implications for vocal production. J Exp Biol *218*,
1102 991-998.
1103 Rimoin, D.L., and Edgerton, M.T. (1967). Genetic and clinical heterogeneity in the oral-
1104 facial-digital syndromes. J Pediatr *71*, 94-102.
1105 Rinon, A., Lazar, S., Marshall, H., Buchmann-Moller, S., Neufeld, A., Elhanany-Tamir,
1106 H., Taketo, M.M., Sommer, L., Krumlauf, R., and Tzahor, E. (2007). Cranial neural crest
1107 cells regulate head muscle patterning and differentiation during vertebrate
1108 embryogenesis. Development *134*, 3065-3075.
1109 Roberts, L.H. (1975a). Functional anatomy of the rodent larynx in relation to audible and
1110 ultrasonic cry production. Zool J Linn Soc *56*, 255-264.
1111 Roberts, L.H. (1975b). The rodent ultrasound production mechanism. Ultrasonics *13*, 83-
1112 88.
1113 Ryan, M.J. (1985). The túngara frog, A study in sexual selection and communication
1114 (Chicago: University of Chicago Press).
1115 Ryan, M.J.D.R.C. (1990). Vocal Morphology of the Physalaemus-Pustulosus Species
1116 Group Leptodactylidae Morphological Response to Sexual Selection for Complex Calls.
1117 Biological Journal of the Linnean Society *40*, 37-52.
1118 Sacchi, R., Galeotti, P., Fasola, M., and Gerzeli, G. (2004). Larynx morphology and
1119 sound production in three species of Testudinidae. J Morphol *261*, 175-183.
1120 Saga, Y., Miyagawa-Tomita, S., Takagi, A., Kitajima, S., Miyazaki, J., and Inoue, T.
1121 (1999). MesP1 is expressed in the heart precursor cells and required for the formation of
1122 a single heart tube. Development *126*, 3437-3447.
1123 Sakoe, H., and Chiba, S. (1978). Dynamic-Programming Algorithm Optimization for
1124 Spoken Word Recognition. Ieee T Acoust Speech *26*, 43-49.
1125 Sales, G., and Pye, D. (1974). Ultrasonic communication by animals (New York: Halsted
1126 Press (Wiley)).
1127 Sambasivan, R., Kuratani, S., and Tajbakhsh, S. (2011). An eye on the head: the
1128 development and evolution of craniofacial muscles. Development *138*, 2401-2415.
1129 Sanders, I., Weisz, D.J., Yang, B.Y., Fung, K., and Amirali, A. (2001). The mechanisms
1130 of ultrasonic vocalization in the rat. Soc Neurosci Abstr *27*, 241.
1131 Sanudo, J.R., and Domenech-Mateu, J.M. (1990). The laryngeal primordium and
1132 epithelial lamina. A new interpretation. J Anat *171*, 207-222.
1133 Sefton, E.M., Piekarski, N., and Hanken, J. (2015). Dual embryonic origin and patterning
1134 of the pharyngeal skeleton in the axolotl (Ambystoma mexicanum). Evol Dev *17*, 175-
1135 184.

Sewell, G.D. (1970). Ultrasonic Communication in Rodents. Nature *227*, 410-&.
Siebert, J.R., Graham, J.M., Jr., and MacDonald, C. (1985). Pathologic features of the CHARGE association: support for involvement of the neural crest. Teratology *31*, 331-336.
Silengo, M.C., Bell, G.L., Biagioli, M., and Franceschini, P. (1987). Oro-facial-digital syndrome II. Transitional type between the Mohr and the Majewski syndromes: report of two new cases. Clin Genet *31*, 331-336.
Steichen-Gersdorf, E., Gassner, I., Covi, B., and Fischer, H. (1994). Oral-facial-digital syndrome II. Transitional type between Mohr and Majewski syndrome: report of a new case with congenital stenosis of the trachea. Clin Dysmorphol *3*, 245-250.
Stevens, C.A., and Ledbetter, J.C. (2005). Significance of bifid epiglottis. Am J Med Genet A *134*, 447-449.
Tabler, J.M., Barrell, W.B., Szabo-Rogers, H.L., Healy, C., Yeung, Y., Perdiguero, E.G., Schulz, C., Yannakoudakis, B.Z., Mesbahi, A., Wlodarczyk, B.*, et al.* (2013). Fuz mutant mice reveal shared mechanisms between ciliopathies and FGF-related syndromes. Dev Cell *25*, 623-635.
Tabler, J.M., Rice, C.P., Liu, K.J., and Wallingford, J.B. (2016). A novel ciliopathic skull defect arising from excess neural crest. Dev Biol *417*, 4-10.
Tenenbaum, J.B., de Silva, V., and Langford, J.C. (2000). A global geometric framework for nonlinear dimensionality reduction. Science *290*, 2319-+.
Thomas, L.B., Stemple, J.C., Andreatta, R.D., and Andrade, F.H. (2009). Establishing a new animal model for the study of laryngeal biology and disease: an anatomic study of the mouse larynx. J Speech Lang Hear Res *52*, 802-811.
Toriyama, M., Lee, C., Taylor, S.P., Duran, I., Cohn, D.H., Bruel, A.L., Tabler, J.M., Drew, K., Kelly, M.R., Kim, S.*, et al.* (2016). The ciliopathy-associated CPLANE proteins direct basal body recruitment of intraflagellar transport machinery. Nat Genet *48*, 648-656.
Tyler, D.C. (1985). Laryngeal cleft: report of eight patients and a review of the literature. Am J Med Genet *21*, 61-75.
Van Daele, D.J., and Cassell, M.D. (2009). Multiple forebrain systems converge on motor neurons innervating the thyroarytenoid muscle. Neuroscience *162*, 501-524.
van der Maaten, L., and Hinton, G. (2008). Visualizing Data using t-SNE. J Mach Learn Res *9*, 2579-2605.
Vaux, K.K., Wojtczak, H., Benirschke, K., and Jones, K.L. (2003). Vocal cord abnormalities in Williams syndrome: a further manifestation of elastin deficiency. Am J Med Genet A *119A*, 302-304.
Walsh, D.M., Shalev, S.A., Simpson, M.A., Morgan, N.V., Gelman-Kohan, Z., Chemke, J., Trembath, R.C., and Maher, E.R. (2013). Acrocallosal syndrome: identification of a novel KIF7 mutation and evidence for oligogenic inheritance. Eur J Med Genet *56*, 39-42.
Watts, C.R., Awan, S.N., and Marler, J.A. (2008). An investigation of voice quality in individuals with inherited elastin gene abnormalities. Clin Linguist Phon *22*, 199-213.
Yamada, W., Nagao, K., Horikoshi, K., Fujikura, A., Ikeda, E., Inagaki, Y., Kakitani, M., Tomizuka, K., Miyazaki, H., Suda, T.*, et al.* (2009). Craniofacial malformation in R-spondin2 knockout mice. Biochem Biophys Res Commun *381*, 453-458.
Young, B.A., Sheft, S., and Yost, W. (1995). Sound production in Pituophis melanoleucus (Serpentes: Colubridae) with the first description of a vocal cord in snakes. J Exp Zool *273*, 472-481.
Zippelius, H.M., and Schleidt, W.M. (1956). Ultraschall-Laute Bei Jungen Mausen. Naturwissenschaften *43*, 501-501.

1187
1188

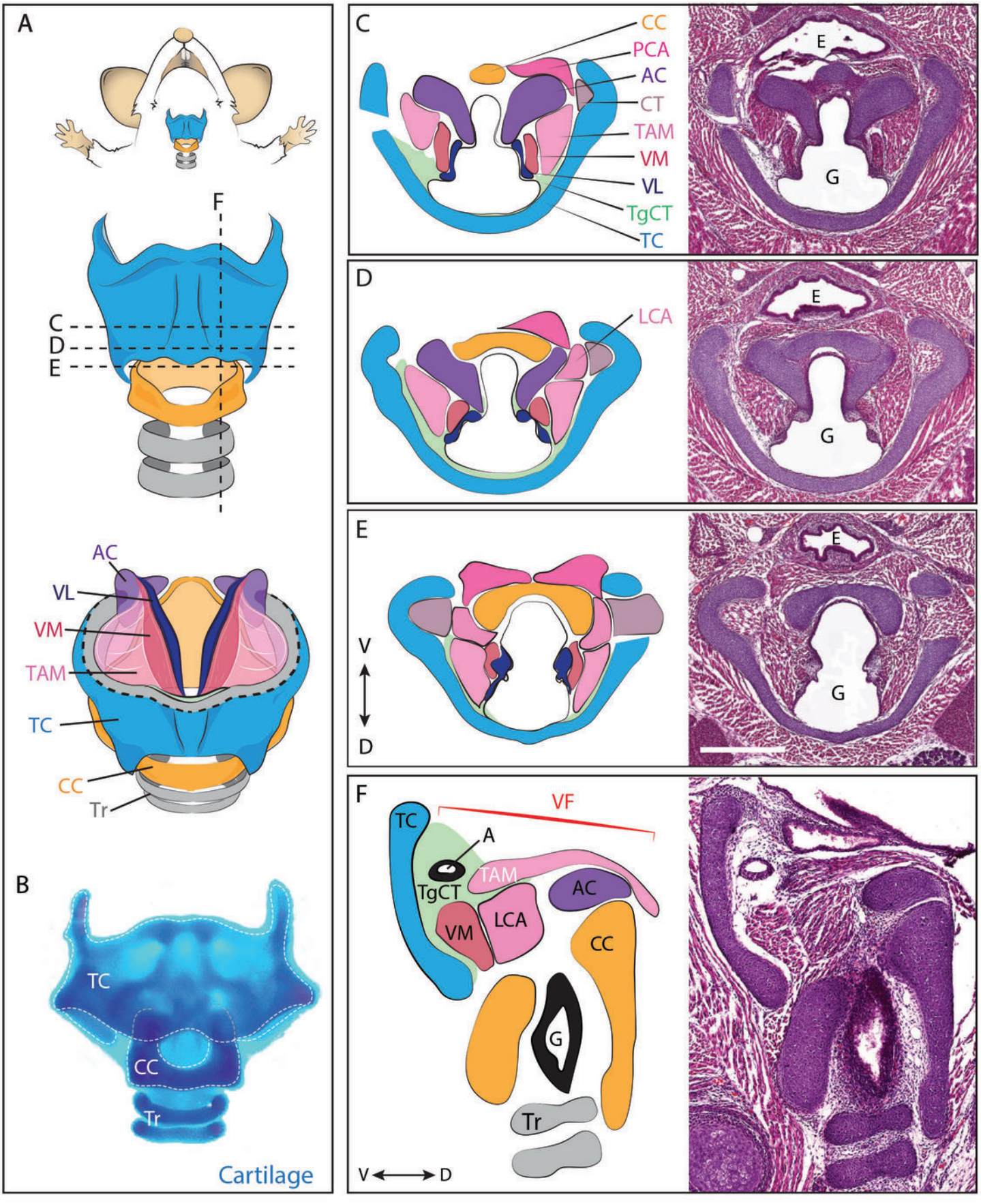

Tabler and Rigney et al.
Figure 1

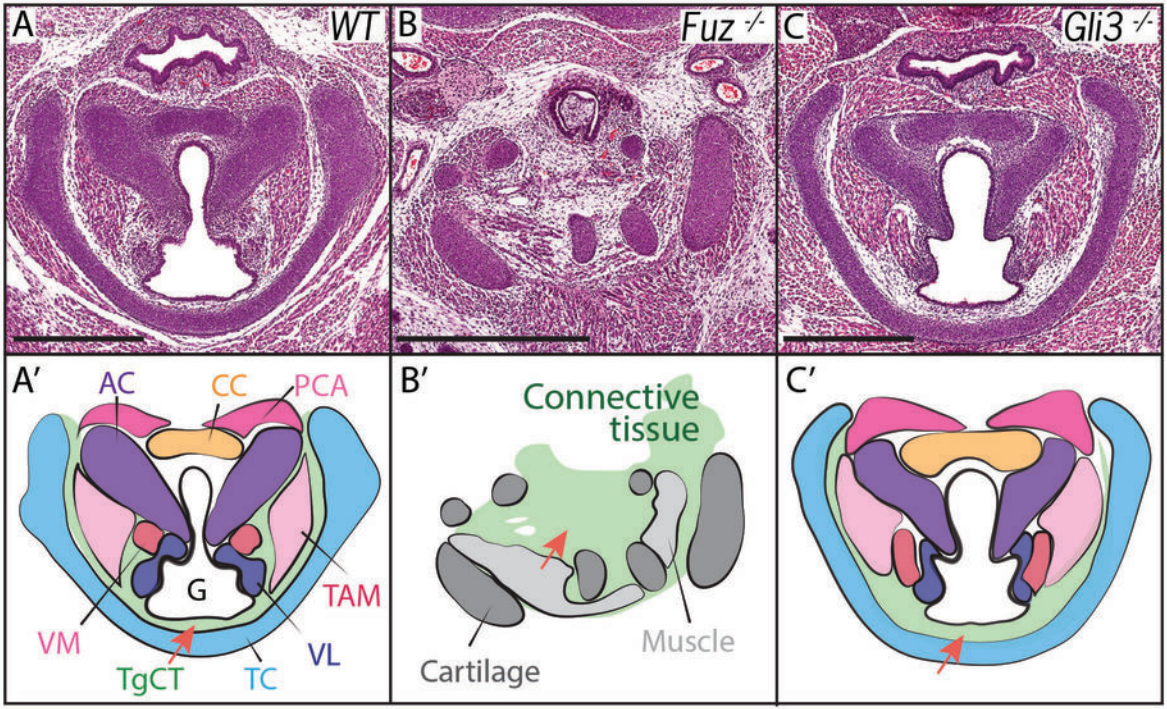

Tabler and Rigney et al.
Figure 2

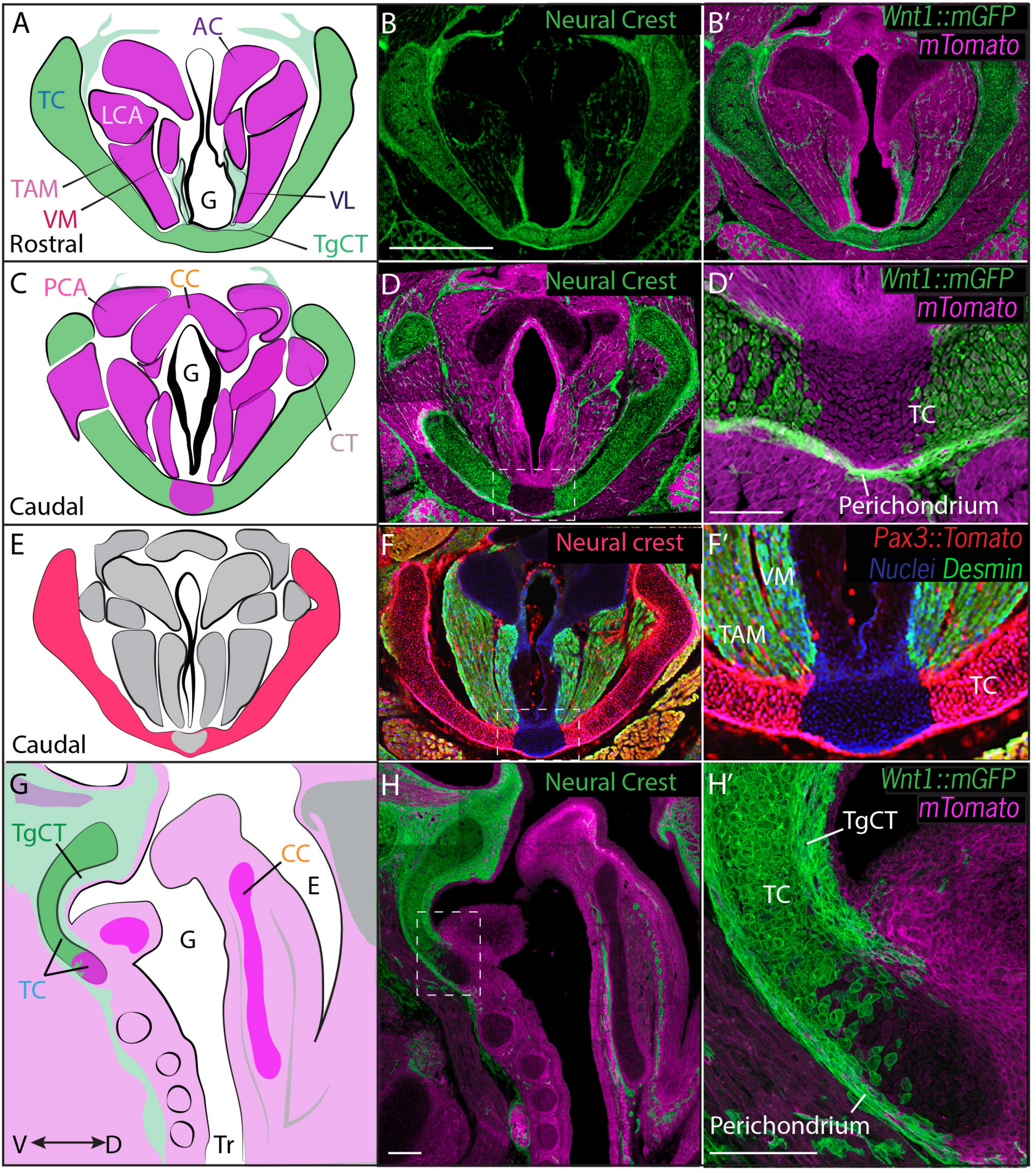

Tabler and Rigney et al.
Figure 3

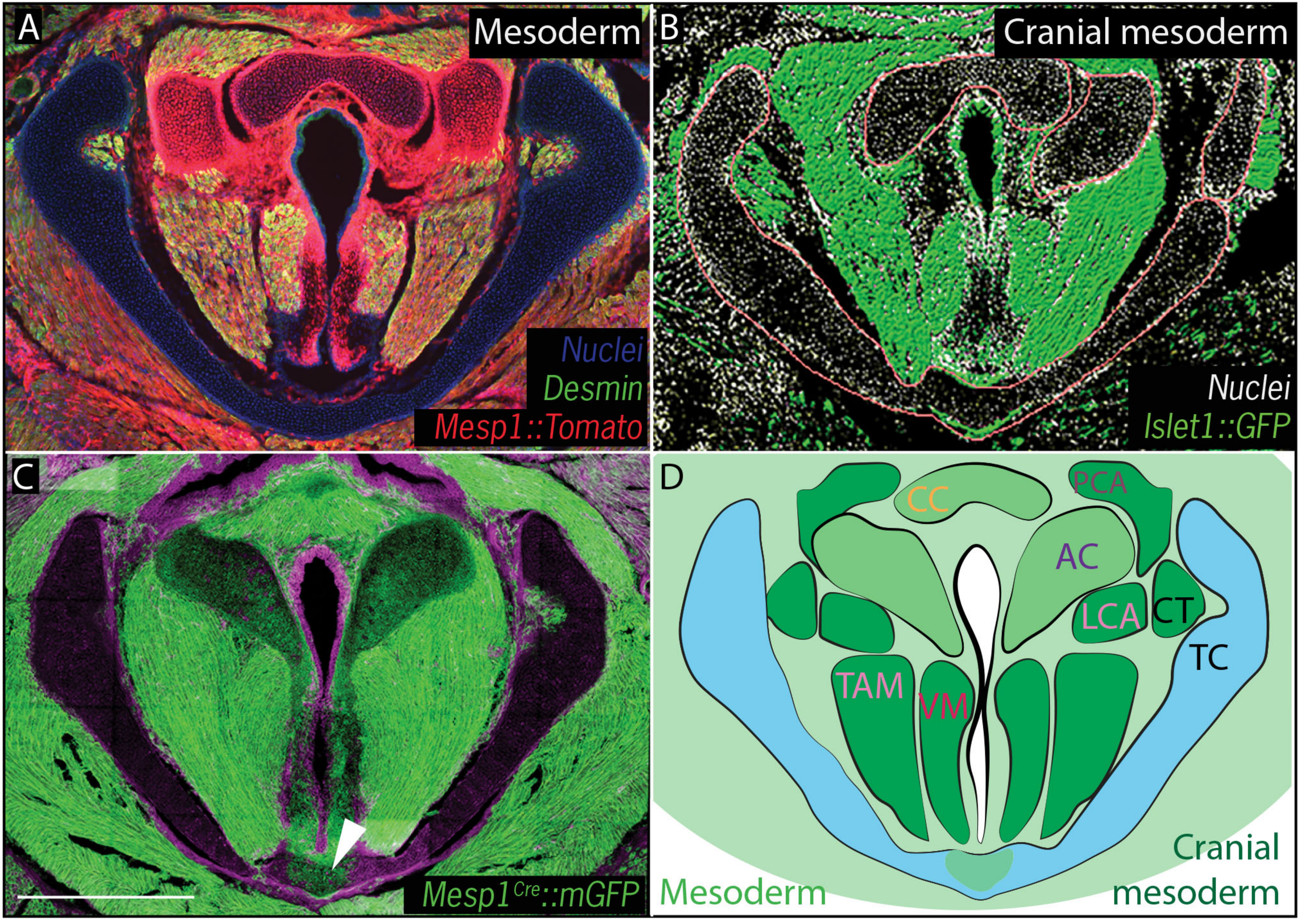

Tabler and Rigney et al.
Figure 4

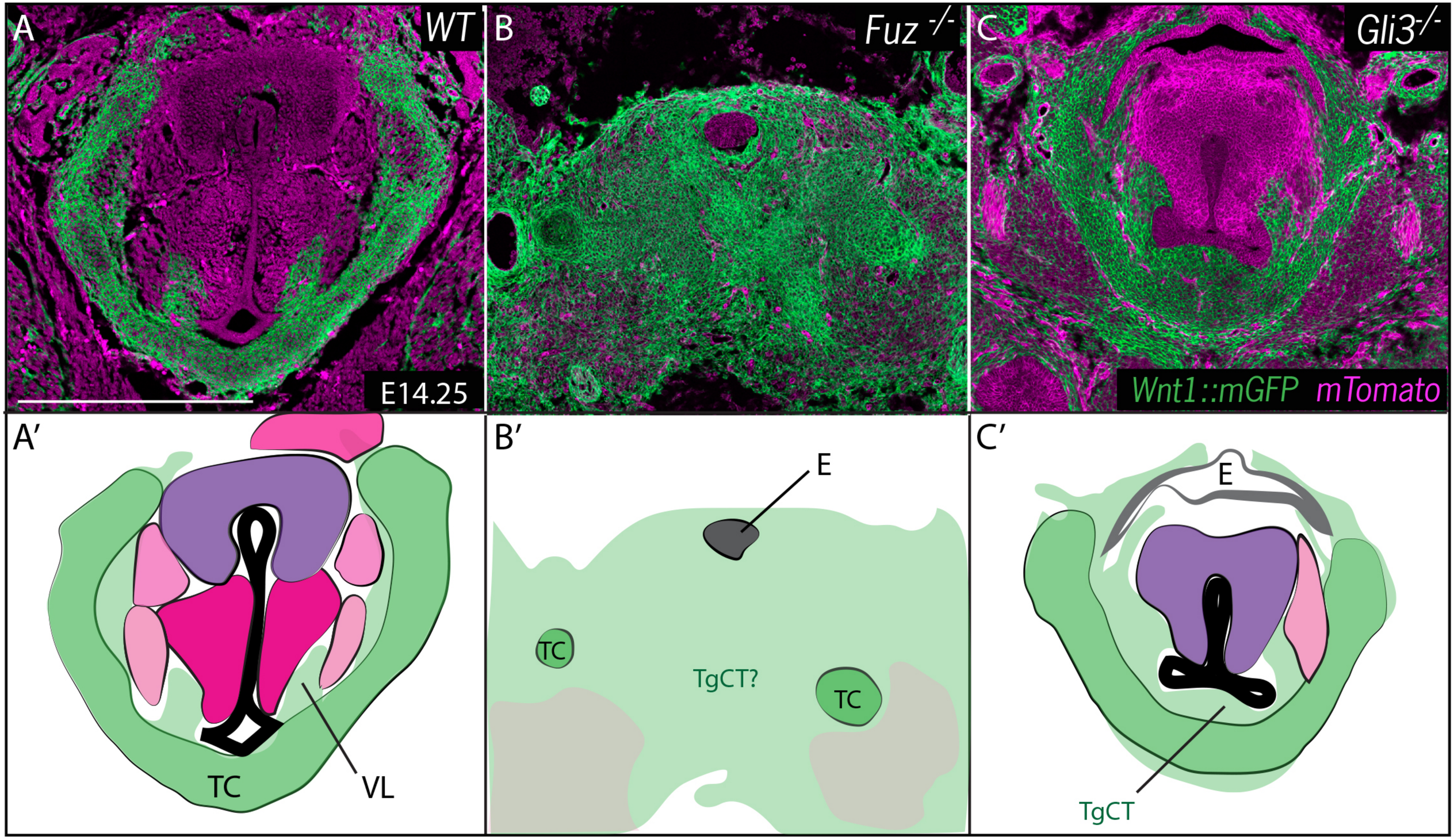

Tabler and Rigney et al.
Figure 5

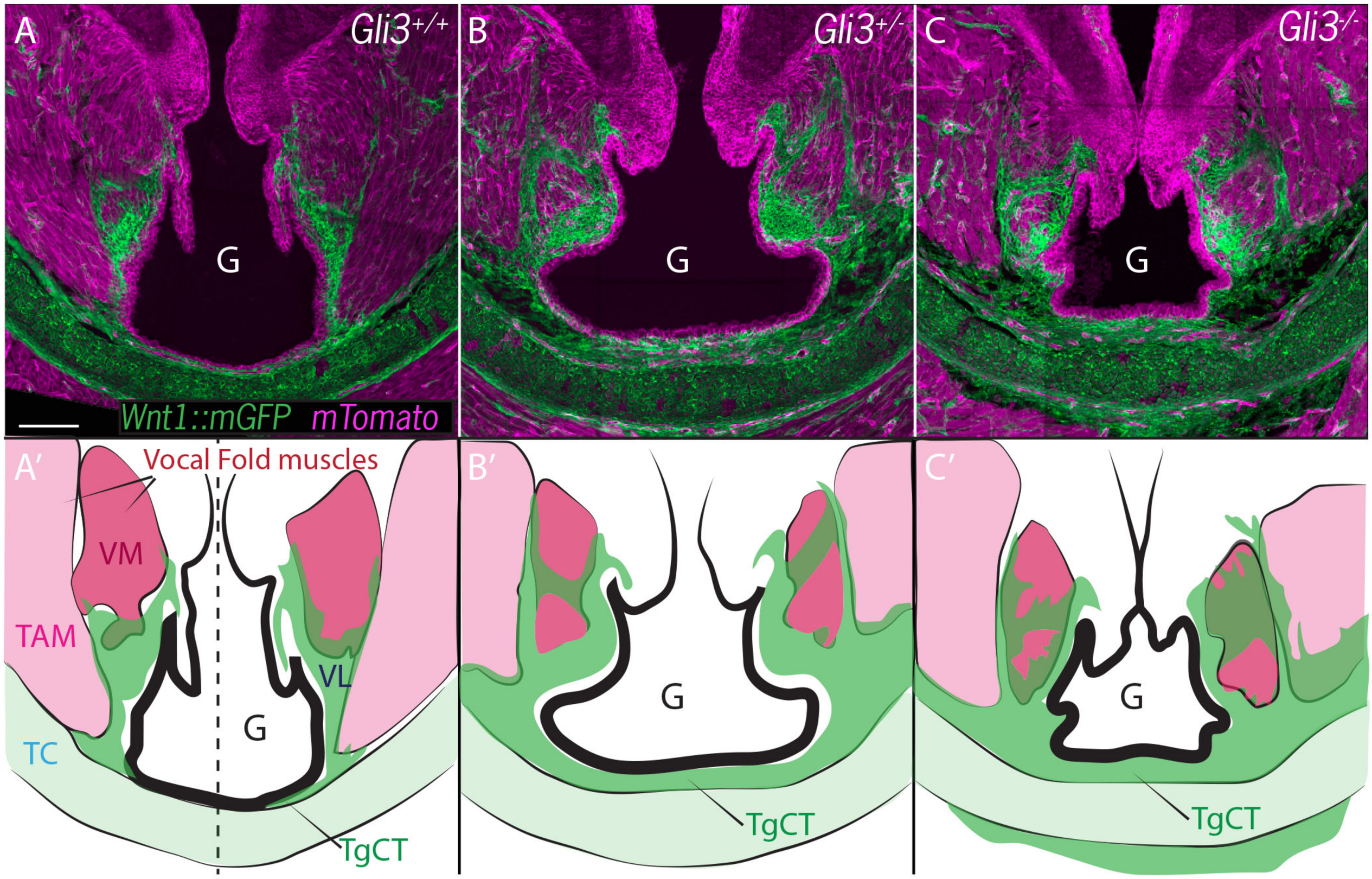

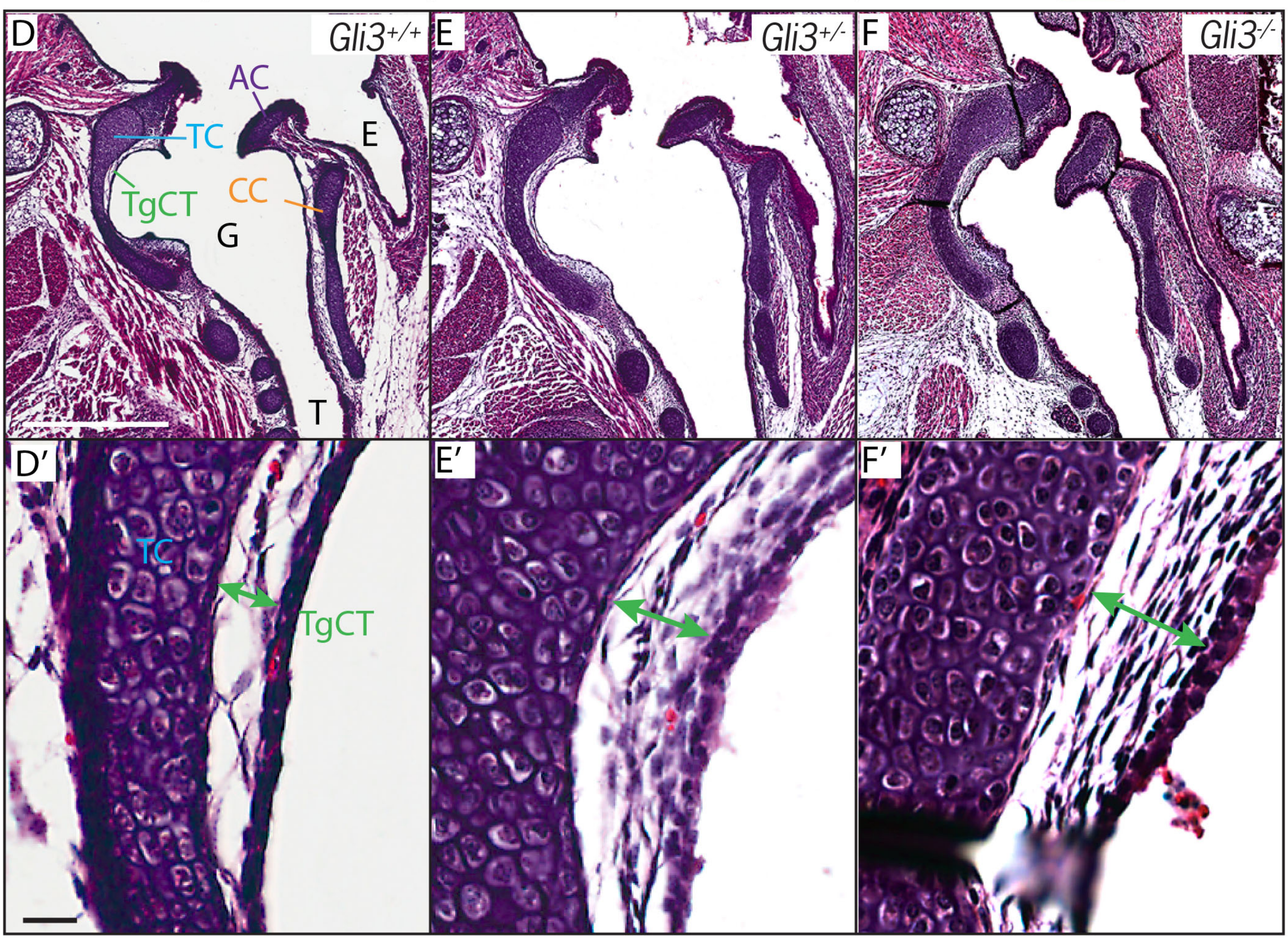

Tabler and Rigney et al.
Figure 6

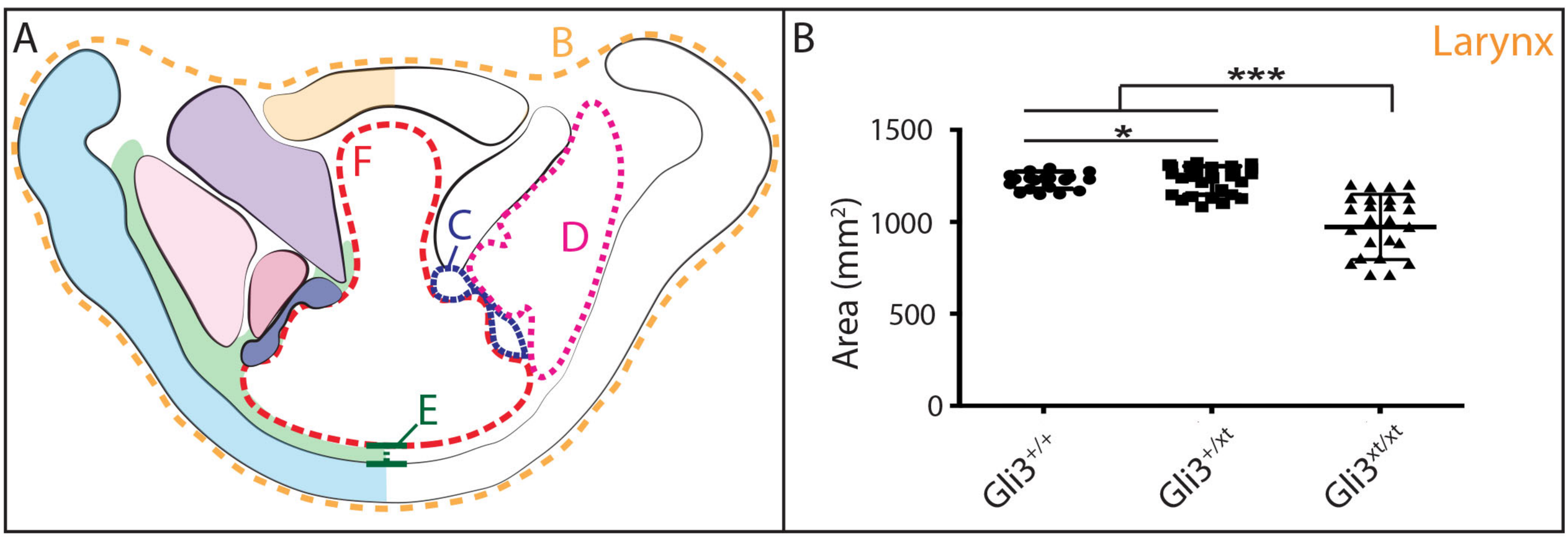

Tabler and Rigney et al.
Figure 7

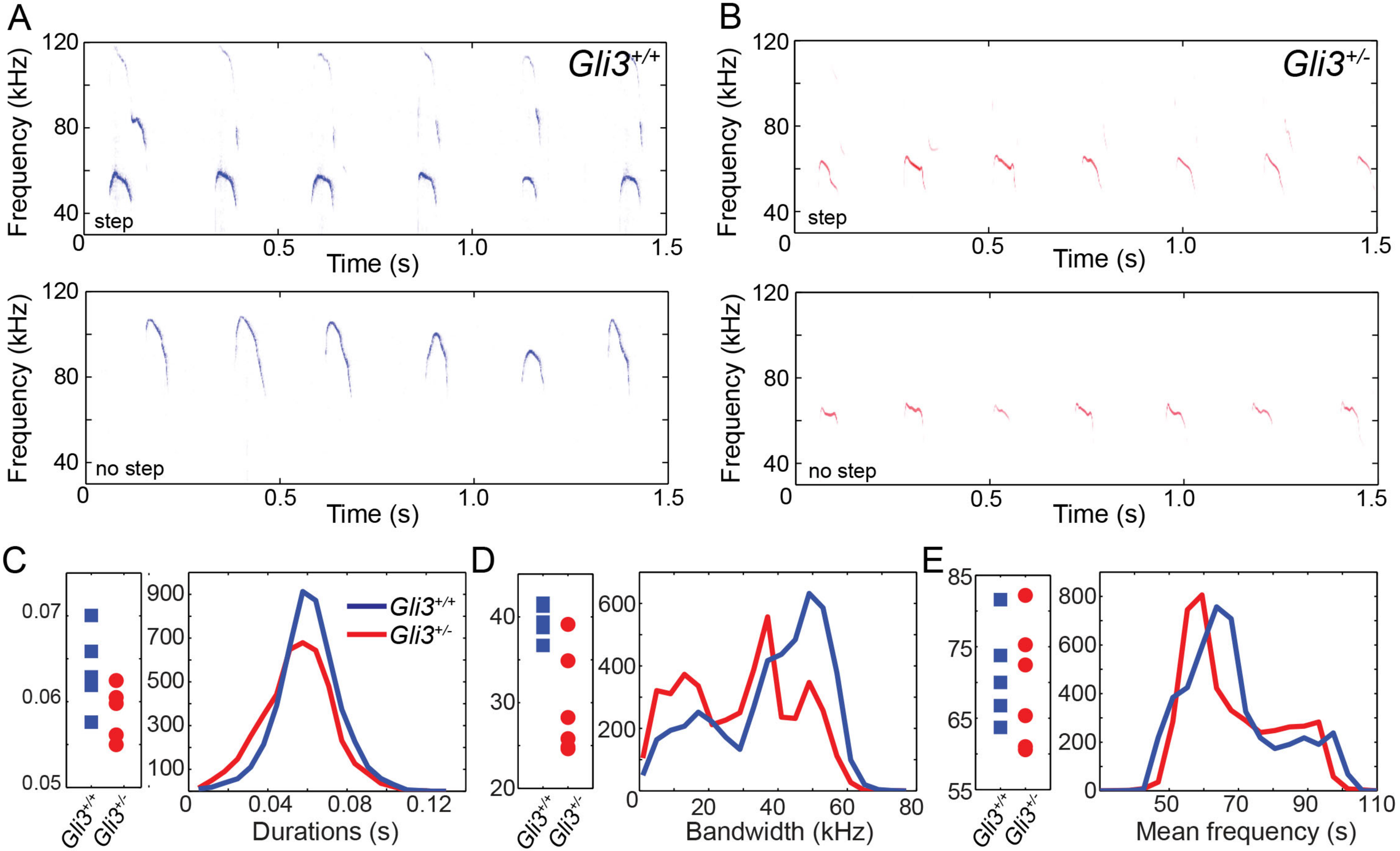

Tabler and Rigney et al.
Figure 8

A Individual vocalisations

B Total vocalisation density map

C Frequency contour distributions

n=618

n=379

n=391

n=549

n=1132

n=530

n=926

n=454

n=984

n=591

n=181

n=194

n=848

n=763

Step

No Step

D $Gli3^{+/+}$

E $Gli3^{+/-}$

F Difference

x10^{-5}

5
4
3
2
1
0
-1
-2
-3
-4
-5

Tabler and Rigney et al.
Figure 9

A

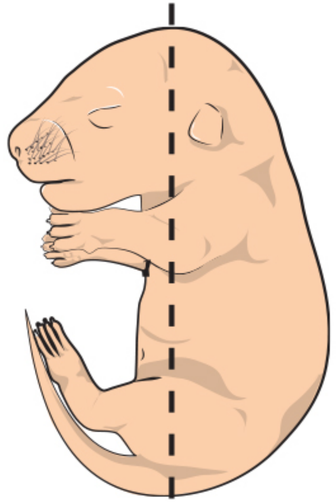

B $Fuz^{+/+}; Fgf8^{Lacz/+}$

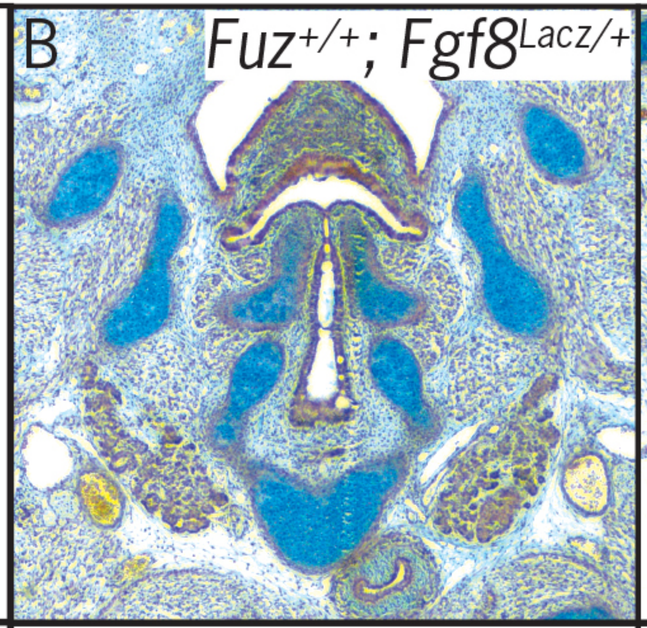

C $Fuz^{-/-}$

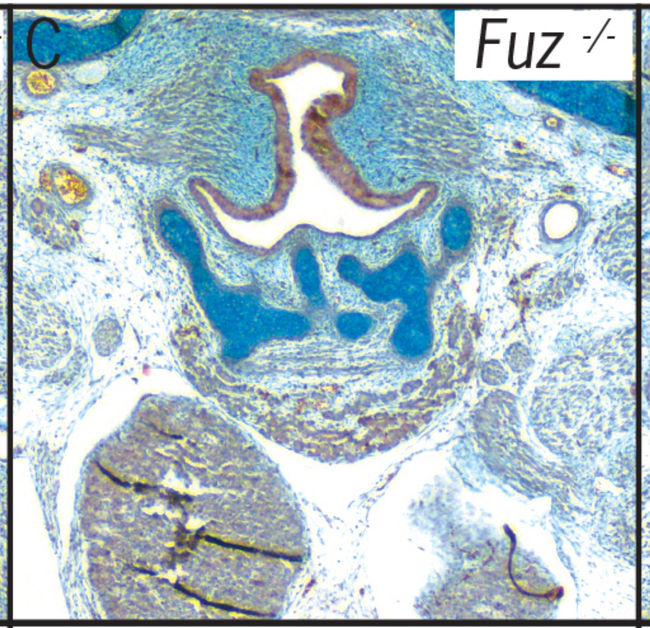

D $Fuz^{-/-}; Fgf8^{Lacz/+}$

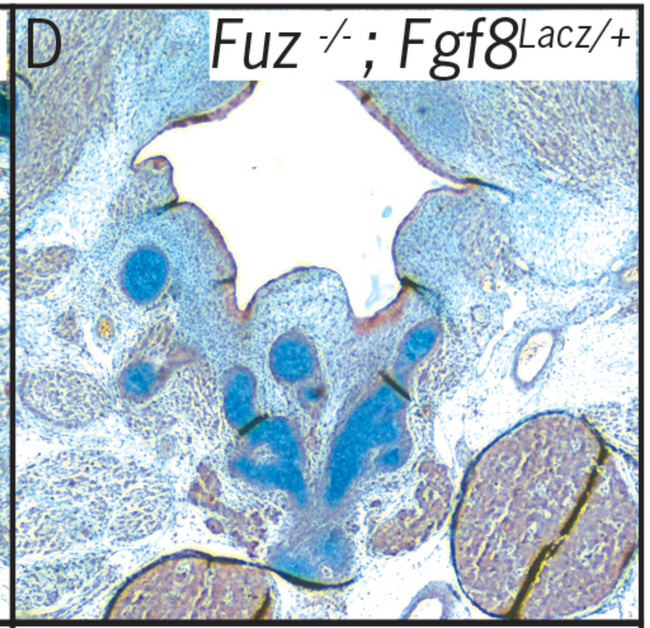

Hyoid

Thyroid

Arytenoid

Cricoid

Glottis

Oesophagus

B'

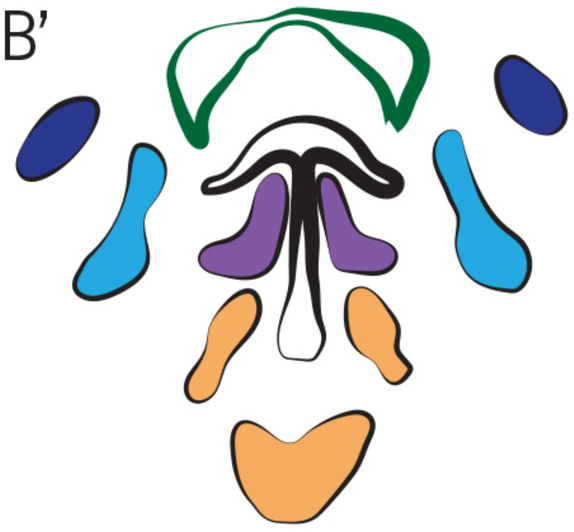

C'

D'

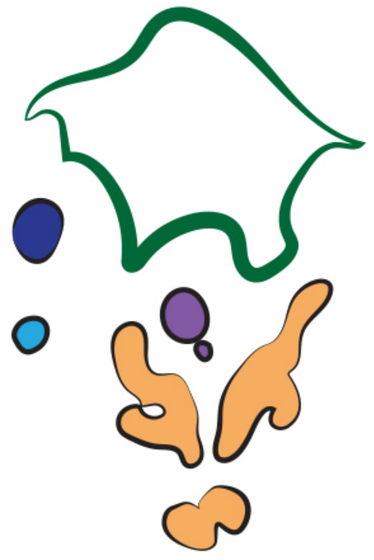

Tabler and Rigney et al. 2016
Supplemental Figure 1

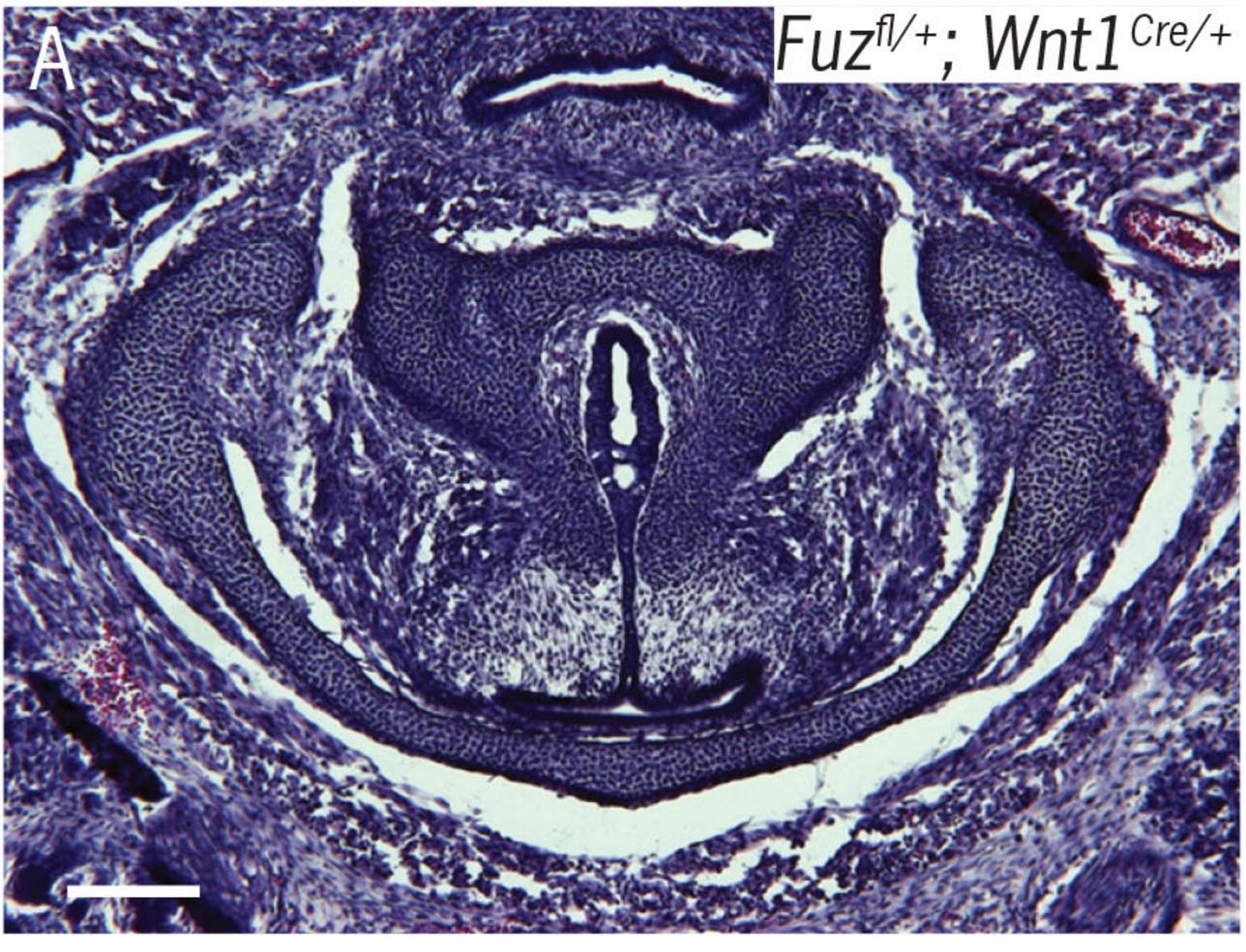

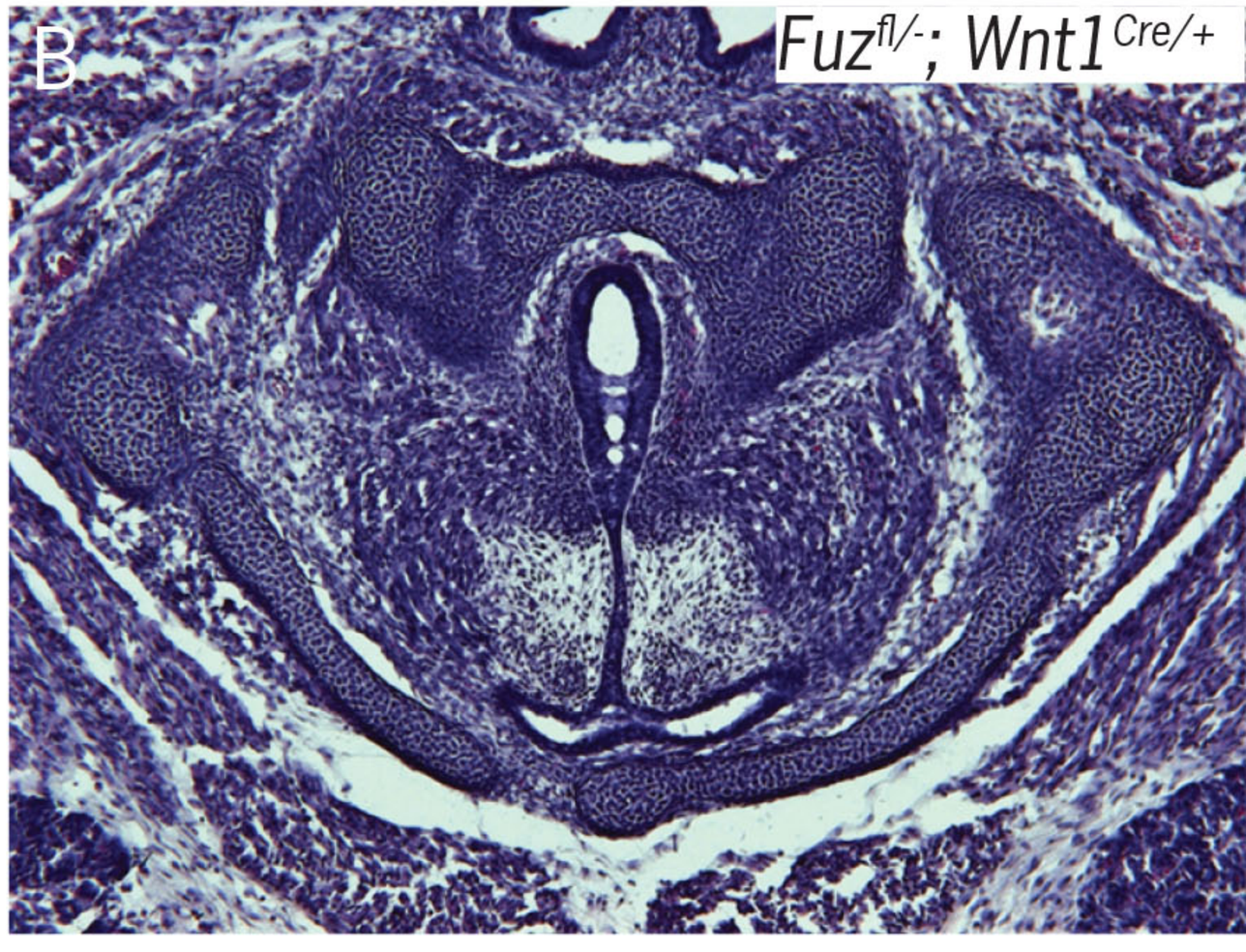

Tabler and Rigney et al. 2016

Supplemental Figure 2